NEUROSCIENCE

Selective reactivation of value- and place-dependent information during sharp-wave ripples in the intermediate and dorsal hippocampus

Seung-Woo Jin†, Hee-Seung Ha, Inah Lee*

Reactivating place cells during sharp-wave ripples in the hippocampus is important for memory consolidation. However, whether hippocampal reactivation is affected by the values of events experienced by the animal is largely unknown. Here, we investigated whether place cells in the dorsal (dHP) and intermediate hippocampus (iHP) of rats are differentially reactivated depending on the value associated with a place during the learning of places associated with higher-value rewards in a T-maze. Place cells in the iHP representing the high-value location were reactivated significantly more frequently than those representing the low-value location, characteristics not observed in the dHP. In contrast, the activities of place cells in the dHP coding the routes leading to high-value locations were replayed more than those in the iHP. Our findings suggest that value-based differential reactivation patterns along the septotemporal axis of the hippocampus may play essential roles in optimizing goal-directed spatial learning for maximal reward.

INTRODUCTION

The hippocampus plays a critical role in episodic memory (*1*–*3*), which often consists of events associated with different values occurring in space. In the hippocampus, highly synchronized activities of place cells are entrained during sharp-wave ripples (SWRs), and the firing sequences during recent wakeful experiences are reexpressed during SWRs (*4*). These findings have given rise to the hypothesis that the reactivation of place cells contributes to the consolidation process by transferring the newly obtained hippocampal information to neocortical networks (*5*).

It is important to note that prior studies focused mostly on investigating the sequential firing patterns of place cells in the dorsal hippocampus (dHP). For example, it has been demonstrated that an animal's recent navigational traces or upcoming paths leading to a goal location are reactivated ("replayed") in the dHP during SWRs (*6*, *7*). What is largely unknown is whether such reactivations are modulated by different values associated with places. Also, if such value-dependent differential reactivation does occur in the hippocampus, does it occur differentially across different subregions along the longitudinal axis of the hippocampus? A previous study reported that SWRs and replay events occur more frequently in the dHP when a larger reward is provided (*8*). Another study showed that the routes associated with larger rewards are replayed more in the dHP than those with smaller rewards (*9*). However, whether such value-based modulation of replay also occurs in other hippocampal regions is still largely unknown.

In our previous study, we found that the place fields of place cells in the intermediate hippocampus (iHP) were immediately remapped in response to a change in value at a reward location in the T-maze, coalescing around the location associated with the higher-value reward rather than the lower-value reward (*10*). Other researchers have reported that a subset of place cells in the iHP are dedicated to coding reward information by remapping their fields to a new place where a reward is available (*11*, *12*). Therefore, the place cells activated in the dHP and iHP during a navigation task in which places are differentiated by different reward values may also be reactivated differentially during SWRs. We hypothesize that, in the iHP, the neural activities of place cells representing higher-value locations are reactivated more than those representing lower-reward locations and that such neural firing characteristics may not occur in the dHP, as suggested by our prior study (*10*).

To test the above hypothesis, we simultaneously recorded neural activities from single units in the dHP and iHP, while rats performed a place-preference task on a T-maze (*10*). We found that place cells in the iHP representing higher-value locations were reactivated more frequently than those coding lower-value locations. However, this value-dependent reactivation pattern was not observed in the dHP. Instead, precise spatial trajectories that sequentially lead to the goal locations were replayed in the dHP, whereas no sequential replay was observed in the iHP. This double dissociation between the iHP and dHP suggests that functionally heterogeneous information content is reactivated during SWRs in different hippocampal regions when goal-directed navigation requires differentiating places based on their values.

RESULTS

Behavioral performance in the place-preference task

Rats ($n = 6$) were trained in a place-preference task on a T-maze (Fig. 1A and movie S1). Briefly, in block 1, rats were required to find the high-value reward arm (HiV-arm) against the low-value reward arm (LoV-arm) by trial and error (Fig. 1A) until they reached the learning criterion. To encourage hippocampal-based learning and discourage adopting a response strategy (*13*), in block 2, rats were started from the opposite side of the original starting point used in block 1. The spatial relationships between the arms and their reward values were then reversed in block 3, requiring rats to update the place and its value information (Fig. 1A). Spiking activities were recorded from single units in the hippocampus, while rats performed the task. Single-unit recordings were also obtained when rats

Department of Brain and Cognitive Sciences, Seoul National University, Gwanak-ro 1, Gwanak-gu, Seoul 08826, Korea.
*Corresponding author. Email: inahlee@snu.ac.kr
†Present address: Department of Psychiatry and Behavioral Sciences, University of Washington, 1959 N.E. Pacific St, Seattle, WA 98195, USA.

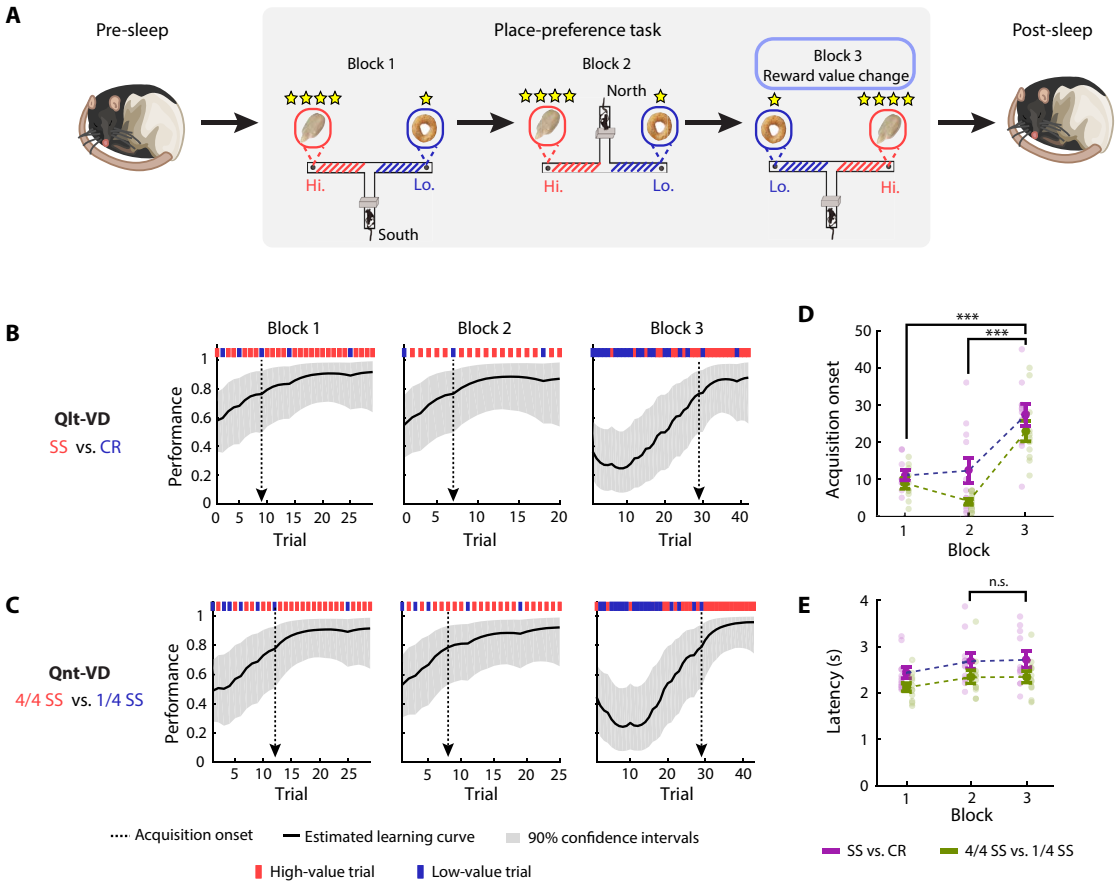

Fig. 1. Behavioral performance during the place-preference task. (**A**) Illustration of the place-preference task protocol. Rats started from the end of the south arm or north arm and were isolated at the ends of arms by an acrylic blocker between inter-trial intervals (ITIs). The arms associated with high-value rewards and low-value rewards were reversed in block 3 (blue shaded box). (**B** and **C**) Behavioral performance graph of sunflower seed (SS) versus Cheerios (CR) session (rat 473 – session 2) and $^{4}/_{4}$ SS versus $^{1}/_{4}$ SS session (rat 473 – session 3), based on a state-space model (*14*). High-value and low-value trials are marked by red and blue lines, respectively, above the learning curve. The solid black line indicates the estimated learning curve, and the black dashed line indicates the acquisition onset trial, calculated by the state-space model. The 90% confidence interval of the learning curve is shown by gray shading. (**D**) Boxplot for trials that reached acquisition onset for each block. (**E**) Boxplot presentation of mean latency per block [(D) and (E) $N = 22$ sessions]. ***$P < 0.001$. n.s., not significant.

were asleep or immobile before and after the place-preference task (approximately 30 min per sleep session).

Reward values were manipulated both qualitatively and quantitatively in our study. Specifically, in sessions 1 and 2 (i.e., qualitative value-differentiation session, or Qlt-VD), a quarter of sunflower seed (SS) and a quarter of a Cheerios were used as high- and low-value rewards, respectively (Fig. 1B). In sessions 3 and 4 (i.e., quantitative value-differentiation session, or Qnt-VD), whole SS and a quarter of a SS were used as high- and low-value rewards, respectively (Fig. 1C). To estimate the trial in which the rat learned the HiV-arm (acquisition onset) in each block, we applied a state-space model to behavioral performance data (*14*). Compared to blocks 1 and 2, learning took place slower in block 3 ($P < 0.001$ for both blocks 1 and 2 versus block 3 in Fig. 1D; Wilcoxon signed-rank test with Bonferroni corrections) (Fig. 1D). This difference reflected the fact that rats continually visited the LoV-arm because that arm had been baited with high-value rewards in previous blocks. The delayed onset of acquisition in block 3 compared to block 2 cannot be ascribed to a decrease in motivation because their latencies were similar between blocks 2 and 3 ($P = 0.21$ for block 2 versus block 3 in Fig. 1E; Wilcoxon signed-rank test). Because the shape of the estimated learning curve and the timing (i.e., trial) of acquisition onset were similar between Qlt-VD and Qnt-VD, neural signals recorded from the two types of sessions were pooled in subsequent analyses.

More frequent occurrence of reward zone–associated SWRs in the iHP than in the dHP

Single-unit spiking activities ($n = 769$ in iHP and $n = 569$ in dHP) and local field potentials (LFPs) were simultaneously recorded from the dHP and iHP, defined as in our previous study (*10*), while rats performed the place-preference task. The SWRs (150 to 250 Hz) used for analysis were recorded from CA1 pyramidal cell layers in the dHP and iHP (fig. S1, A and B). SWRs were characterized by large amplitudes (>4 SDs) and coactivation of at least 5% of cells recorded in a given session, while rats showed minimal movement (Fig. 2, A and B, and fig. S2, A and B; see Materials and Methods for details). Putative inhibitory interneurons were excluded from subsequent analyses (fig. S1C). Most putative complex spike cells were recorded from the CA1 (fig. S1D).

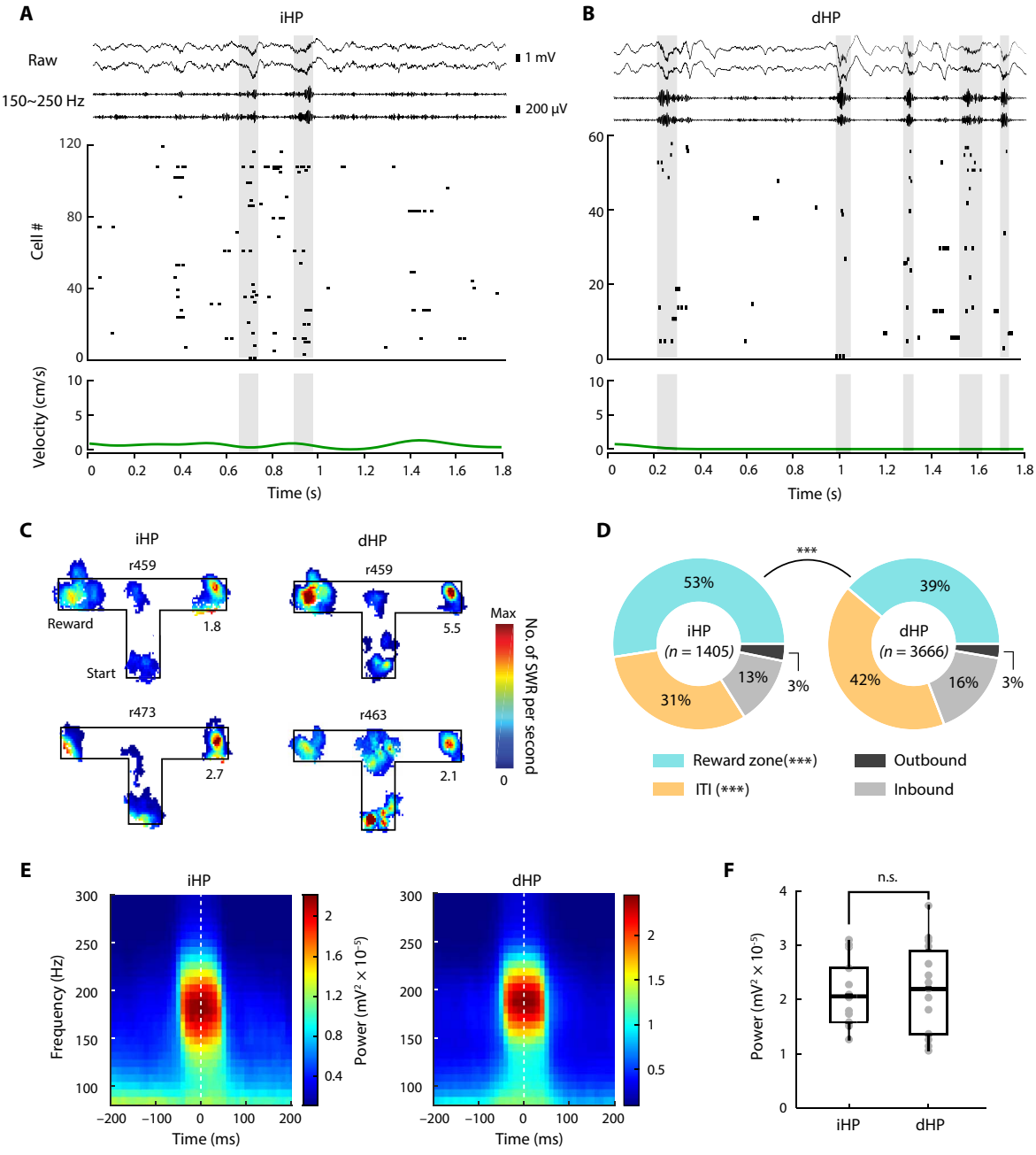

Fig. 2. Detection of SWRs during the place-preference task. (**A** and **B**) Graphs of raw LFP, 150- to 250-Hz filtered signal, ensemble firing, and velocity illustrating the SWR periods that satisfied SWR criteria. SWR periods recorded from the iHP (A) and dHP (B) are indicated by gray-shaded areas. See also fig. S1. The scale indicates the amplitude of raw and filtered LFP signals. (**C**) Results for two individual rats exemplifying the distribution of SWR occurrence in the iHP and dHP. The black line indicates the contour of the maze; a spatial bin with lower SWR rates was excluded from the color display. SWRs recorded from blocks 1 and 3 were pooled for calculation of the SWR rate map. Peak SWR rates (in hertz) were annotated below each rate map. See also fig. S2. (**D**) Pie chart showing the frequency of SWRs recorded from the dHP and iHP when rats were in the outbound zone, reward zone, inbound zone, and ITI zone during a place-preference task (N_{iHP} = 1405 and N_{dHP} = 3666 SWRs). (**E**) Spectrogram displaying the frequency and power of SWR, aligning with the time of SWR peak amplitude. (**F**) Comparison of the peak power of SWR between the iHP and dHP (N_{iHP} and N_{dHP} = 15 sessions). ***$P < 0.001$.

On the basis of our SWR detection criteria, we detected 1405 and 3666 SWR events from the iHP and dHP, respectively, in the entire session (Fig. 2D). A majority of SWR events (approximately 80 to 85%) took place when rats were in reward zones consuming the reward or during inter-trial interval (ITI) periods, while rats waited for the next trial across block 1 to 3 (Fig. 2, C and D, and fig. S2, A to C). Similar proportions of SWRs occurred between the reward zone and ITI period in the dHP (Fig. 2D). However, approximately half of SWR events in the iHP occurred while rats were in the reward zone, suggesting that the effect of the reward on the occurrence

of SWRs was more pronounced in the iHP compared to the dHP ($P < 0.001$ for group comparison; $P < 0.001$ for reward zone and ITI conditions; chi-square test with Bonferroni corrections) (Fig. 2D). In addition, the properties of SWRs occurring within the reward zones, including their frequency and power, exhibited similar characteristics in both the dHP and iHP ($P = 0.95$ for power between iHP and dHP; Wilcoxon rank-sum test) (Fig. 2, E and F). Since we are mostly interested in the reward value-related neural reactivation in the dHP and iHP, we restrict our analysis of SWR events to the reward zones ($n = 737$ in iHP and $n = 1424$ in dHP), reflecting the high likelihood of a substantial disparity in the proportion of SWR events within these zones between the dHP and iHP. In the reward zone, the ripple rate was greater in blocks 2 and 3 than in block 1 in both the dHP and iHP. The increase in the ripple rate may be attributable to the allocentric spatial strategy in block 2 and to the value reversal learning in block 3 (fig. S2D).

Previous studies showed that SWRs in the dHP and iHP could occur either locally or globally (*15*, *16*). We also found local and global SWRs both in the dHP and iHP (fig. S2E). Consistent with the previous studies (*15*), SWRs that occurred in the iHP (32.8 ± 4.1%) were more likely to co-occur with dHP SWR (21.8 ± 2.7%) ($P < 0.05$; one-sample *t* test; fig. S2F). Also, we found that synchronized SWRs comprise approximately 40% of the global SWRs. However, the SWRs recorded in the dHP led those in the iHP in 35% of SWRs, and the opposite temporal relationship was found in 23% (fig. S2, G and H). A prior study reported that iHP-leading SWRs were more dominant than dHP-leading ones (*16*). This difference may be ascribed to the difference in behavioral paradigms. That is, we used a dorsal hippocampal-dependent task, whereas Patel and colleagues (*16*) used a foraging task in an open field.

Selective increase of the high–value-coding place cells during nonspatial reactivation in the correct trials in the iHP but not in the dHP

It is well known that place cells representing the goal arms may undergo global remapping by the animal's past trajectories (i.e., retrospective coding) (*17*, *18*). Consistent with the previous literature (*17*) where 68.8% ($n = 121$ of 176) of place cells in the dHP remapped globally in response to the changes in the starting position, we found that 55.3 and 39.9% of place cells in the dHP and iHP, respectively, remapped globally between blocks 1 and 2 (fig. S1E). Thus, to investigate the effect of the value reversal on place fields while minimizing the retrospective coding in our analysis, we compared the spatial rate maps between blocks 1 and 3 because animals started from the south starting arms in both blocks. During the acquisition of reversed reward contingency, some place fields maintained their place representations, irrespective of changes in reward value, suggesting their primary role in encoding spatial information. On the other hand, certain fields underwent global remapping toward the arms associated with either high-value or low-value rewards, indicating a substantial influence of reward value on these cells' spatial representations (Fig. 3A). The degree of alteration in spatial firing patterns following the reversal of reward contingency was measured by Pearson's correlation coefficients between the rate maps before (i.e., block 1) and after the reward reversal (i.e., block 3). If coefficients exceeded 0.75, then we designated them as location-coding place cells (Location-cells), assuming that they had stable representations regardless of the reward contingency. Depending on the locations of place fields in block 3, $\text{Location}_{\text{HiV}}$-cells and $\text{Location}_{\text{LoV}}$-cells were further classified (Fig. 3, A-a and C-a).

In contrast, when the coefficients fell below 0.75, these place cells were classified as spatial value-coding cells. We further divided the value-coding cells into HiV-cells and LoV-cells based on the post-learning rate maps in block 3. Because animals might consider a high-value location a low-value one or are unsure of the value associated with locations, we only used the post-learning trials when classifying the HiV- and LoV-cells. If the place fields of post-learning rate maps were in the HiV-arm and LoV-arm, then we categorized them as high–value-coding place cells (HiV-cells) (Fig. 3, A-b and C-b) and low–value-coding place cells (LoV-cells) (Fig. 3, A-c and C-c), respectively. After rats learned the HiV-arm and LoV-arm, their behavior was inevitably biased toward the HiV-arm during learning. However, they visited the LoV-arm one to three times in most sessions (fig. S1F), and we classified LoV-cells using a small number of trials. Therefore, the LoV-cells' field size was smaller than the HiV-cells, presumably due to the sampling issue. Nonetheless, their place representation was similar to that of the HiV cells (Fig. 3, B and D). In addition, the place cells whose fields included the stem of the maze were classified as stem-coding cells (stem cells), and this cell type may be important in decision-making. Because these five cell types were activated during navigation from the start to the reward zone, we included them in our main analysis.

The proportion of five cell types was similar between iHP and dHP ($P = 0.96$; chi-square test). The proportion of HiV-cells and LoV-cells was not statistically different in both the iHP ($n = 27$ and 26 for HiV-cells and LoV-cells, respectively; $P = 0.92$ for one-sample chi-square test) and dHP ($n = 22$ and 23 for HiV-cells and LoV-cells, respectively; $P = 0.92$), suggesting that value-coding place cells are uniformly distributed in both HiV- and LoV-arms (Fig. 3E). HiV-cells and LoV-cells were subdivided into two classes: "Turn-on" cells were the place cells that were silent in block 1 but became turned on in either HiV-arm or LoV-arm in block 3 (place cells in the first and second rows of Fig. 3, A, b and c; and C, b and c). "Shift" cells were the place cells whose firing fields shifted from a reward location or stem in block 1 to either HiV-arm or LoV-arm in block 3 to encode the value of an arm (place cells in the third and fourth rows in Fig. 3, A, b and c; and C, b and c). HiV-cells and LoV-cells (63 and 61.5%, respectively) in the iHP were Shift cells (fig. S3A). In the dHP, 68.2 and 59.1% of HiV-cells and LoV-cells, respectively, were Shift cells (fig. S3B). The proportions of Shift and Turn-on cells were not significantly different between HiV-cells and LoV-cells in the iHP ($P = 0.91$; chi-square test) and the dHP ($P = 0.61$; chi-square test). The proportions of these two cell types were similar between the dHP and iHP ($P = 0.82$; chi-square test) (fig. S3, A and B). Because Shift and Turn-on cells had similar reactivation patterns during SWR (fig. S3, C and D), the data from the two types were combined for further analysis.

Next, we investigated how five types of place cells were differentially reactivated during reversal learning for reward contingency in block 3 (Fig. 4A). We counted how many times one place cell was reactivated during SWR events (i.e., nonspatial reactivation or NSR henceforth). NSR should not be equated with conventional replay [i.e., spatial replay (SR)] because NSR does not require spatial reactivation of place cells during SWR events. We computed NSR separately in HiV and LoV reward zones, and the ripple rates (in hertz) in the reward zone were similar between the correct and incorrect trials ($P = 0.52$; Wilcoxon signed-rank test) (Fig. 4D). We first

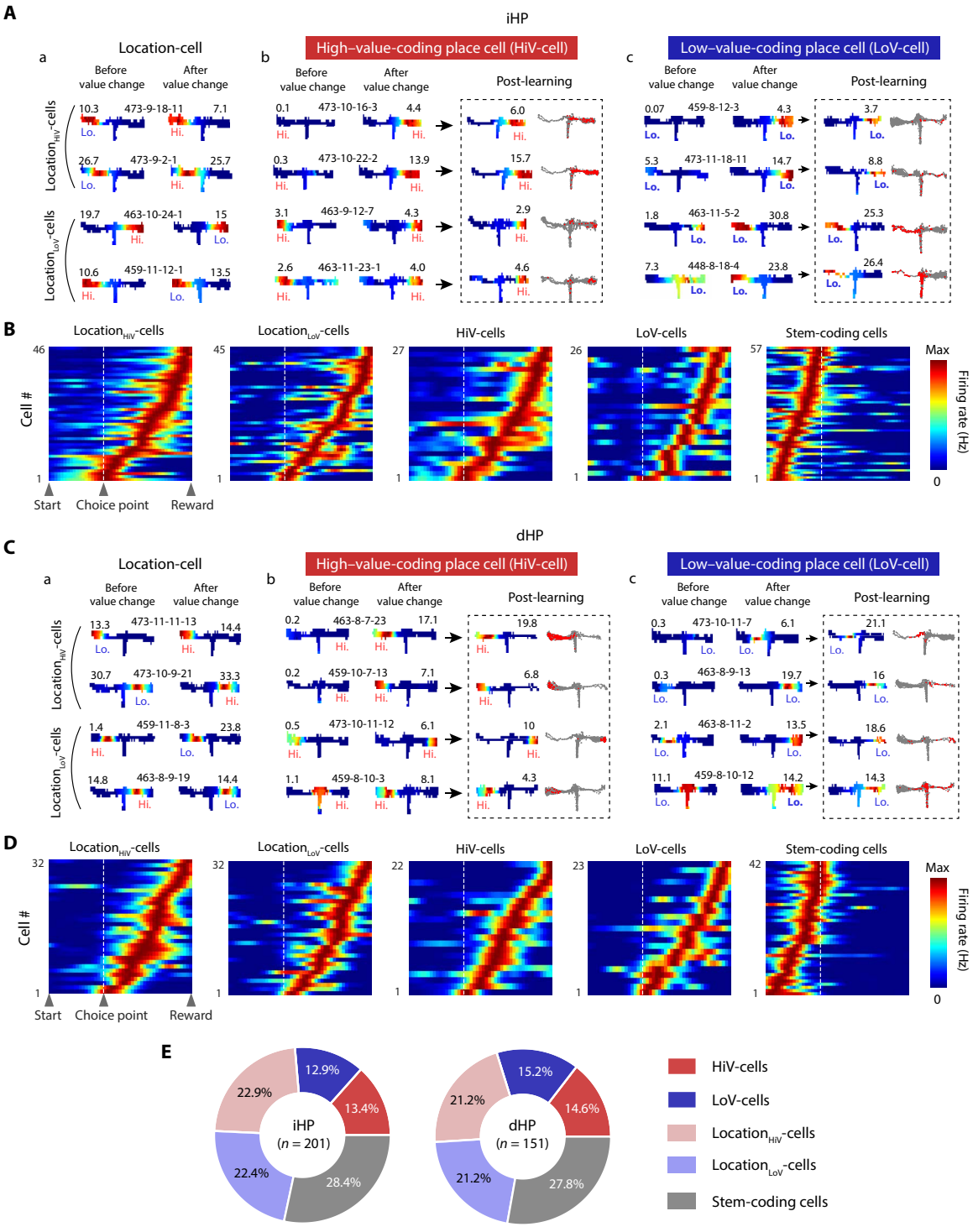

Fig. 3. Classification of place cells into five types. (**A** to **D**) The single-cell examples and population rate maps showing HiV-cell, LoV-cell, Location$_{HiV}$-cell, Location$_{LoV}$-cell, and stem-coding cell. They were recorded from the iHP [(A) and (B)] and the dHP [(C) and (D)]. Cell identity (rat # - session # - tetrode # - cluster #) and peak firing rates (in hertz) were annotated between rate maps and above each rate map, respectively. We used all block 3 trials to make spatial rate maps of before and after value changes. However, only post-learning trials were used in post-learning rate maps and population rate maps [(B) and (D)]. (**E**) Pie chart showing the number of HiV-cell, LoV-cell, Location$_{HiV}$-cell, Location$_{LoV}$-cell, and stem-coding cell recorded from the iHP and the dHP (iHP: $N_{HiV} = 27$, $N_{LoV} = 26$, $N_{LocationHiV} = 46$, $N_{LocationLoV} = 45$, $N_{Stem} = 57$ cells; dHP: $N_{HiV} = 22$, $N_{LoV} = 23$, $N_{LocationHiV} = 32$, $N_{LocationLoV} = 32$, $N_{Stem} = 42$ cells).

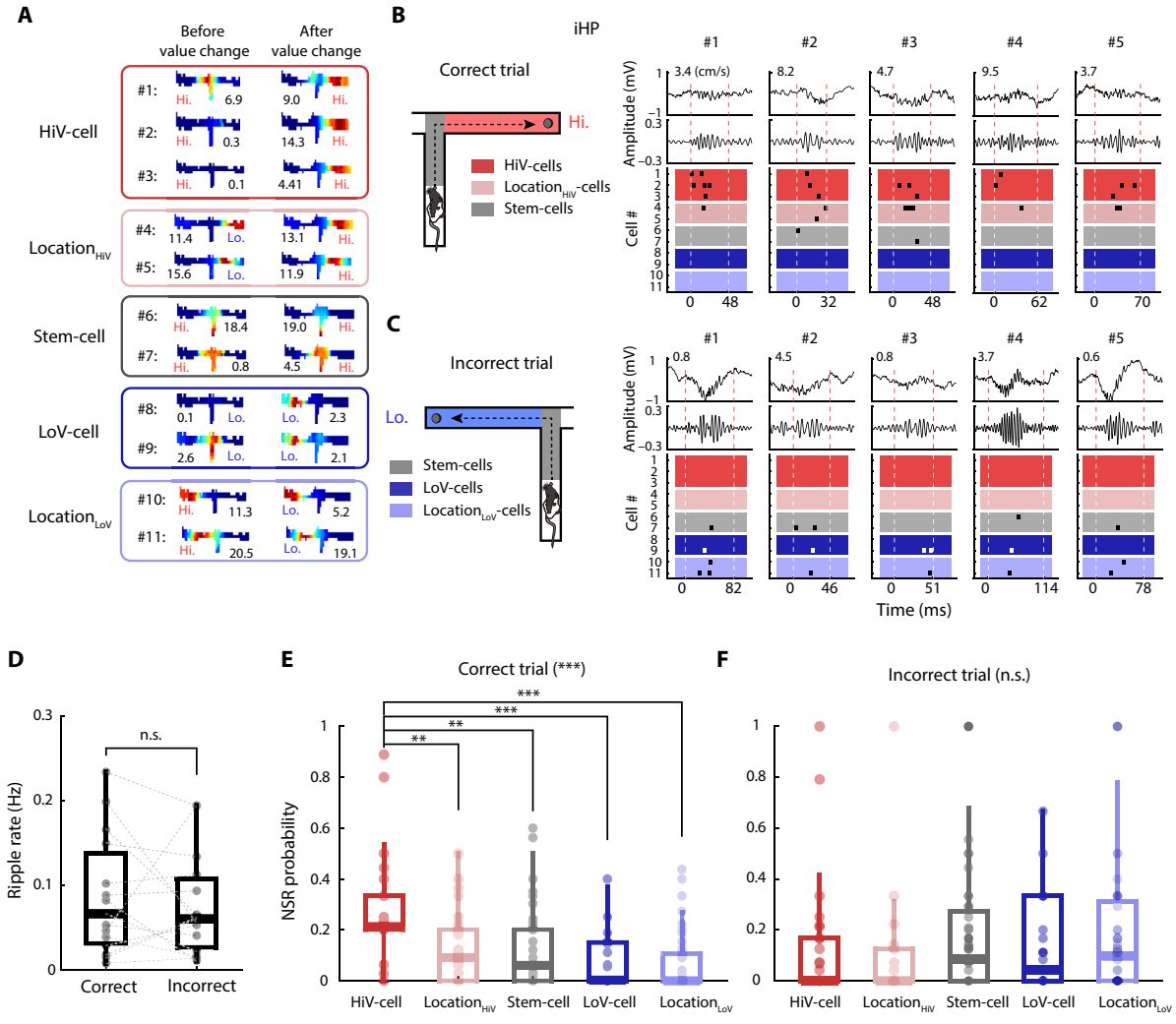

Fig. 4. Selective increase in nonspatial reactivation of HiV-cells than the remaining cell types in the iHP. (**A**) Illustrative examples of spatial rate maps for three cell types in the iHP. Cells #1 to 11 were observed in rat 473 – session 3. Peak firing rates (in hertz) were shown below the rate map, and "Hi." indicated the location of the high-value reward. Spatial rate maps of 11 single cells in the iHP were shown, together with their NSR patterns during awake SWRs in block 3. Spatial rate maps for each type are grouped as denoted by colored boxes. (**B** and **C**) Examples of SWR and NSR activities during reward zone in correct (B) and incorrect trials (C). Raw LFP (top), 150- to 250-Hz filtered signals (middle), and reactivation of cells #1 to 11 (bottom) per SWR period are shown. The mean velocity (in centimeters per second) during an SWR is shown on the raw LFP graph. The dashed line indicates the boundary of an SWR. (**D**) Comparison of reward zone SWR rates between correct and incorrect trials in the iHP ($N_{Correct}$ and $N_{Incorrect}$ = 15 sessions). (**E** and **F**) Comparison of NSR probabilities in the correct (E) and incorrect trials (F). Each data point indicates the NSR probability of a single cell (N_{HiV} = 27, N_{LoV} = 26, $N_{LocationHiV}$ = 46, $N_{LocationLoV}$ = 45, N_{Stem} = 57 cells). See also fig. S3. $^{**}P < 0.01$ and $^{***}P < 0.001$.

examined NSR during SWRs that occurred in the HiV-reward zone. When rats navigated from start to HiV-arms (i.e., correct trial), stem-coding cells, HiV-cells, and Location$_{HiV}$-cells were activated. We found that these recently activated cells were more likely to participate in NSR during SWR occurring in the HiV reward zone than the less-activated cells (i.e., LoV-cells and Location$_{LoV}$-cells) (Fig. 4B). At the population level, HiV-cells, Location$_{HiV}$-cells, and stem-coding cells had a higher NSR probability than LoV-cells and Location$_{LoV}$-cells in correct trials. The NSR probability of HiV-cells was significantly higher than other cell types ($P < 0.001$ for correct trials; Kruskal-Wallis test) ($P < 0.01$ for HiV-cells versus Location$_{HiV}$-cells and stem-coding cells; $P < 0.001$ for HiV-cells versus LoV-cells and Location$_{LoV}$-cells; Wilcoxon rank-sum test with Bonferroni corrections) (Fig. 4E). Similarly, during SWRs in the LoV reward zone, recently activated cells (i.e., stem-coding cells, LoV-cells, and Location$_{LoV}$-cells) tended to fire in NSR than the less-activated cells (i.e., HiV-cells and Location$_{HiV}$-cells) (Fig. 4C). At the population level, the NSR probability of stem-coding cells, LoV-cells, and Location$_{LoV}$-cells is slightly higher than that of HiV-cells and Location$_{HiV}$-cells, but there was no significant difference between the groups ($P = 0.12$ for incorrect trials; Kruskal-Wallis test) (Fig. 4F).

When we applied the same analysis to the dHP as depicted in Fig. 4, it became evident that all cell types exhibited similar levels of NSR during SWRs (Fig. 5, A to C). Although LoV-cells and Location$_{LoV}$-cells were less likely to be activated during the navigation toward the HiV-arm (i.e., correct trials), these cell types were more likely to participate in NSR during SWRs occurred in the HiV

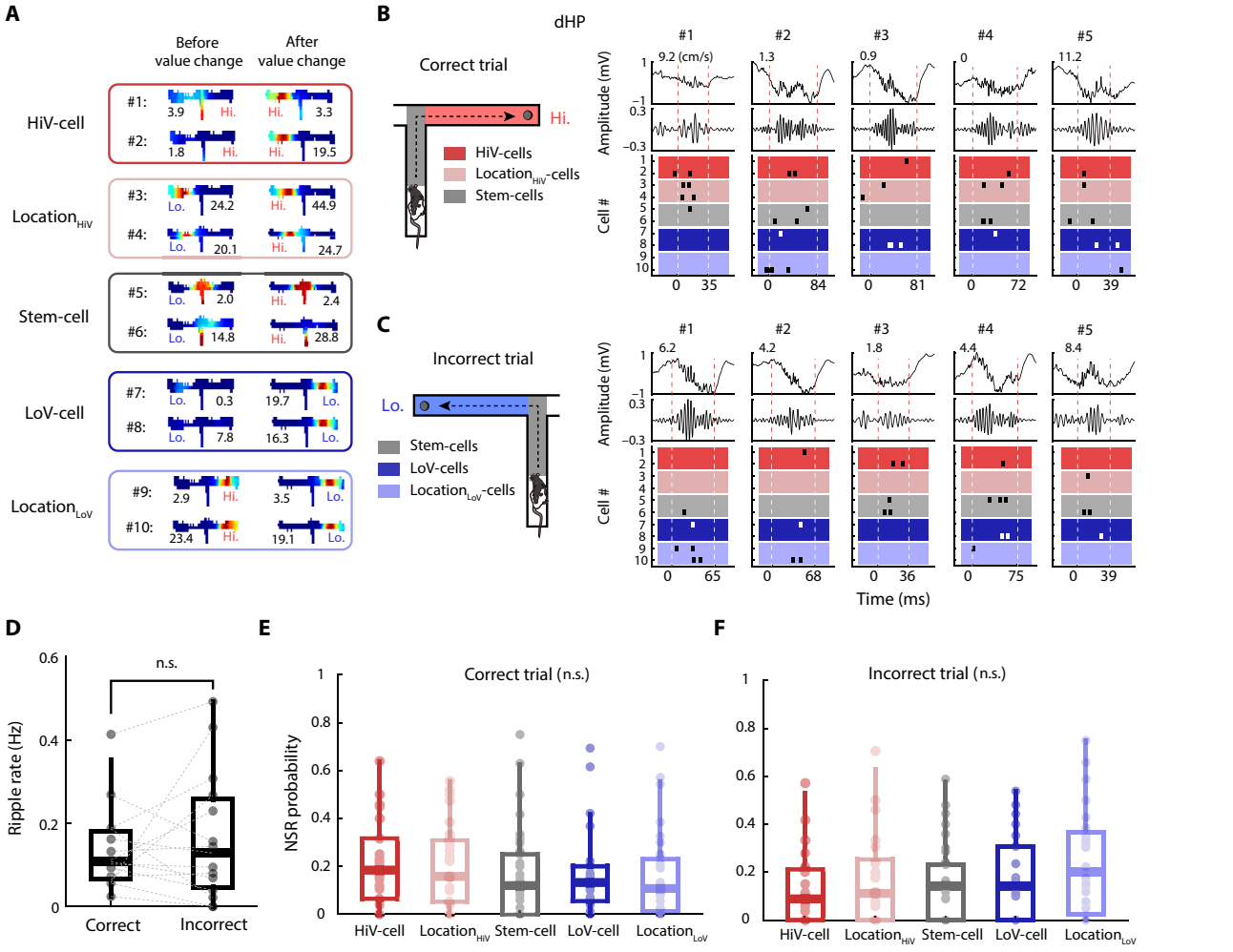

Fig. 5. Uniform reactivation of all cell types in the dHP. (**A**) Illustrative examples of spatial rate maps for three cell types in the dHP. Cells #1 to 10 were observed in rat 463 – session 1. Peak firing rates (in hertz) were shown below the rate map, and "Hi." indicated the location of the high-value reward. Spatial rate maps of 11 single cells in the dHP were shown, together with their NSR patterns during awake SWRs in block 3. Spatial rate maps for each type are grouped as denoted by colored boxes. (**B** and **C**) Examples of SWR and NSR activities during reward zone in correct (B) and incorrect trials (C). Raw LFP (top), 150- to 250-Hz filtered signals (middle), and reactivation of cells #1 to 10 (bottom) per SWR period are shown. The mean velocity (in centimeters per second) during an SWR is shown on the raw LFP graph. The dashed line indicates the boundary of an SWR. (**D**) Comparison of reward zone SWR rates between correct and incorrect trials in the dHP ($N_{Correct}$ and $N_{Incorrect}$ = 15 sessions). (**E** and **F**) Comparison of NSR probabilities in the correct (E) and incorrect trials (F) (N_{HiV} = 22, N_{LoV} = 23, $N_{LocationHiV}$ = 32, $N_{LocationLoV}$ = 32, N_{Stem} = 42 cells). Each data point indicates the NSR probability of a single cell. See also fig. S3.

reward zone (Fig. 5B). Similarly, HiV-cells and Location$_{HiV}$-cells were more involved in NSR during SWRs that occurred in the LoV reward zone (i.e., incorrect trials) (Fig. 5C). We found similar SWRs rates of the dHP between correct and incorrect trials (P = 0.8; Wilcoxon signed-rank test) (Fig. 5D). At the population level, in the correct trials, NSR probability of HiV-cells, Location$_{HiV}$-cells, and stem-coding cells was slightly higher than that of LoV-cells and Location$_{LoV}$-cells, but there was no significant group difference (P = 0.45 for correct trials; Kruskal-Wallis test) (Fig. 5E). Similar NSR trend was also observed in incorrect trials (P = 0.34 for incorrect trials; Kruskal-Wallis test) (Fig. 5F).

This disparity between the dHP and iHP was further confirmed by NSR rates as an alternative measurement (fig. S3, E to H). Notably, the elevated NSR probabilities of HiV-cells in the iHP cannot be attributed to the higher excitability of this cell type, as there was no significant correlation between the peak firing rates of individual place cells and their NSR probabilities (fig. S3I). Therefore, our findings suggest that a selective increase in NSR of place cells representing high-value locations during SWRs is a unique property of the iHP.

Learning-dependent potentiation of nonspatial reactivation of high–value-coding place cells in the iHP but not in the dHP

Next, we investigated whether the NSR of HiV-cells in the iHP was enhanced as rats learned the reversed relationship between place and its associated value in block 3. We used the performance level of 75% as a learning criterion based on the estimation of the acquisition onset computed by a state-space model (Fig. 1, B and C). In the pre-learning stage (i.e., performance <75%), HiV-cells in the iHP

seemed to show a similar level of NSR compared to the other cell types (Fig. 6A, left). However, as rats reached the acquisition onset (i.e., performance >75%), a notable change in NSR patterns occurred; that is, HiV-cells in the iHP were more likely to participate in NSR, whereas $Location_{HiV}$-cells and stem-coding cells in the iHP remained at a similar level of NSR (Fig. 6A, right). We carried out a thorough investigation into learning-dependent alterations in NSR by segregating trials into five-trial bins based on performance (i.e., <50%, 50 to 65%, 65 to 75%, 75 to 90%, and >90%). The results revealed that, before learning (i.e., <50%, 50 to 65%, and 65 to 75%), all cell types showed moderate NSR probability. However, after learning (i.e., 75 to 90% and >90%), HiV-cells exhibited an upsurge in NSR probability, with these cells having a greater NSR probability than other cell types ($P < 0.01$ for 75 to 90%; $P < 0.05$ for >90%; Kruskal-Wallis test) (Fig. 6B). We also confirmed that NSR probability of HiV-cells in the iHP was not potentiated in blocks 1 and 2 compared to block 3 ($P < 0.01$ for block 1 versus 3; $P < 0.05$ for block 2 versus 3; Wilcoxon signed-rank test) (fig. S3J). In contrast, the remaining cell types did not exhibit notable increases in the vicinity of acquisition onset (Fig. 6B).

By subtracting the NSR probability of the pre-learning from the post-learning stage, we further examined the changes in NSR probability before and after the learning of the reversal of reward value. NSR probability of HiV-cells was significantly increased in post-learning compared to the pre-learning stage, whereas that of $Location_{HiV}$-cells, LoV-cells, and $Location_{LoV}$-cells were similar between the two learning stages ($P < 0.05$ for HiV-cells; $P = 0.57$ for $Location_{HiV}$-cells; $P = 0.38$ for LoV-cells; $P = 0.14$ for $Location_{LoV}$-cells; one-sample Wilcoxon signed-rank test with Bonferroni corrections) (Fig. 6C). Stem-coding cells had higher NSR probability in the pre-learning than the post-learning stage ($P = 0.02$; one-sample Wilcoxon signed-rank test), which suggests that decision-related neural reactivation may occur dominantly during the pre-learning stage (Fig. 6C). These findings strongly support the idea that the enhancement of NSR of HiV-cells is contingent on the learning process.

In contrast, when the same analysis was applied to the dHP, we did not observe learning-dependent changes in the reactivation of HiV-cells in the dHP, akin to what was observed in the iHP ($P = 0.79$ for "<50%"; $P = 0.19$ for "50 to 65%"; $P = 0.89$ for "65 to 75%"; $P = 0.102$ for "75 to 90%"; $P = 0.75$ for ">90%"; Kruskal-Wallis test) (Fig. 6, D and E). The relative NSR probability of the post-learning from the pre-learning stage was not statistically different from 0, which suggests that there were no significant changes in NSR patterns in relation to the acquisition of reward reversal learning ($P = 0.31$ for HiV-cells; $P = 0.74$ for $Location_{HiV}$-cells; $P = 0.63$ for stem-coding cells; $P = 0.75$ for LoV-cells; $P = 0.33$ for $Location_{LoV}$-cells; One-sample Wilcoxon signed-rank test with Bonferroni corrections) (Fig. 6F). Collectively, these results suggest that the potentiation of NSR of high–value-coding place cells upon reversal in the iHP may play a critical role in consolidating the newly learned spatial value.

Correlation between the selective reactivation of the place cells in the iHP representing high-value locations during post-learning sleep and the next day's place-value learning

To assess whether the potentiated NSR of HiV-cells in the iHP persists in the post-sleep session following a behavioral recording session, we examined NSR patterns during both pre- and post-sleep sessions, using the same place cells as depicted in Fig. 4. In the pre-sleep session, the frequency of the NSR of HiV-cells in the iHP were similar compared to the remaining cell types (Fig. 7A, left). However, following the behavioral session of the place-preference task, the amount of NSR of HiV-cells was higher than other cell types in the post-sleep session (Fig. 7A, right). Those HiV-cells that exhibited a higher NSR probability during the behavioral session also had a higher NSR probability measured by Δsleep (i.e., subtraction of NSR probability in pre-sleep from that in post-sleep). This observation suggests that potentiated NSR during behavioral sessions was sustained during the post-sleep session ($P < 0.05$, $r^2 = 0.20$; linear regression) (Fig. 7B).

Next, we compared the Δsleep NSR probability among cell types. As we observed in Fig. 7A, the Δsleep NSR probability of HiV-cells was greater than that of remaining cell types in the iHP ($P = 0.011$; Kruskal-Wallis test) ($P < 0.01$ for HiV-cells versus $Location_{HiV}$-cells, LoV-cells, and $Location_{LoV}$-cells; $P < 0.05$ for HiV-cells versus stem-coding cells; Wilcoxon rank-sum test with Bonferroni corrections) (Fig. 7C). The increase in the Δsleep NSR probability of HiV-cells in the iHP exhibited a positive correlation with the learning speed (i.e., the inverse of acquisition onset) in block 1 on the following day ($P < 0.05$, $r^2 = 0.56$; linear regression) (Fig. 7D). Because the response index during pre-learning trials in block 1 was not significantly correlated with the learning speed in block 1 ($P = 0.2$, $r^2 = 0.08$; robust linear regression), the fast-learning speed in block 1 may not be explained solely by the potential response strategy rats might have been using in block 1 (fig. S1G). This result suggests that NSR of HiV-cells in the iHP during post-sleep plays a role in consolidating the high-value location, thereby enhancing spatial learning on the subsequent day.

In contrast, in the dHP, there were no detectable changes of HiV-cells between pre- and post-sleep sessions (Fig. 7E). Specifically, we barely observed a positive correlation between NSR probabilities of HiV-cells during behavioral sessions and sleep ($P = 0.77$, $r^2 = 0.004$; linear regression) (Fig. 7F). In addition, Δsleep NSR probability did not significantly differ among cell types ($P = 0.89$; Kruskal-Wallis test) (Fig. 7G). Furthermore, positive correlations were rarely found between Δsleep NSR probability of HiV-cells and the learning speed of the next day in the dHP ($P = 0.9$, $r^2 = 0.03$; linear regression) (Fig. 7H). We confirmed these findings by conducting separate analyses for the pre- and post-sleep sessions (fig. S4). In addition, the positive relationship in the iHP between the amount of Δsleep NSR probability and learning speed of the next day was not observed in $Location_{HiV}$-cells, LoV-cells, $Location_{LoV}$-cells, and stem-coding cells both in the iHP and dHP (fig. S5). Collectively, our findings imply that the NSR of HiV-cells in the iHP during sleep may underlie the consolidation of value-updated location information.

Spatial replay of place cells leading to the high-value reward location in the dHP but not in the iHP

So far, we have analyzed NSR, focusing on single-cell reactivation during SWRs. From now on, we focus on SR, and it is different from NSR in that we only used SWR events containing four or more place cells that were spatially reactivated. We detected 71 and 185 SWR events from the iHP and dHP, respectively, that met our criterion of the number of place cells (i.e., candidate SR event; see Materials and Methods for details). Although the SR has been widely reported in the dHP in the previous literature (*6*, *7*, *19*), it is largely unknown whether the SR is a phenomenon that appears

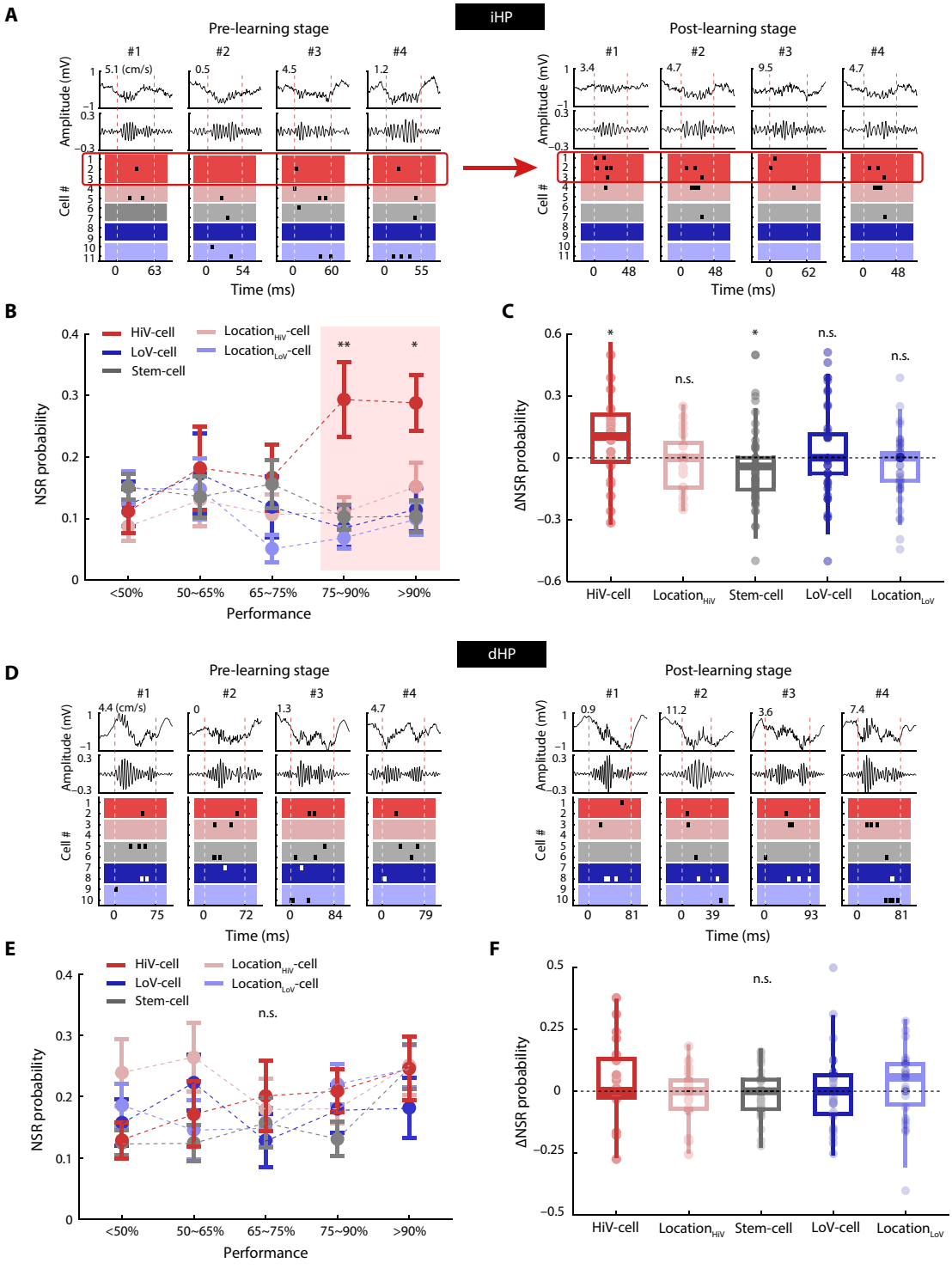

Fig. 6. Learning-dependent changes in the reactivation of HiV-cells in the iHP. (**A**) Illustrative examples of awake SWR and reactivation activities in the iHP that occurred during correct and incorrect trials in the pre-learning state, as well as correct trials in the post-learning state. The cells used in (A) are the same as those in Fig. 4. Spatial rate maps for each type are grouped as denoted by colored boxes. The mean velocity (in centimeters per second) during an SWR is annotated on the raw LFP graph. (**B**) The changes in NSR probability depend on the performance. The correctness was divided into five types. (**C**) Comparison of ΔNSR between pre- and post-learning stages in the iHP among five types of place cells. Each data point denotes the NSR probability of a single cell (N_{HiV} = 27, N_{LoV} = 26, $N_{LocationHiV}$ = 46, $N_{LocationLoV}$ = 45, N_{Stem} = 57 cells). (**D** to **F**) The same analyses as in (A) to (C) were replicated (N_{HiV} = 22, N_{LoV} = 23, $N_{LocationHiV}$ = 32, $N_{LocationLoV}$ = 32, N_{Stem} = 42 cells). *P < 0.05 and **P < 0.01.

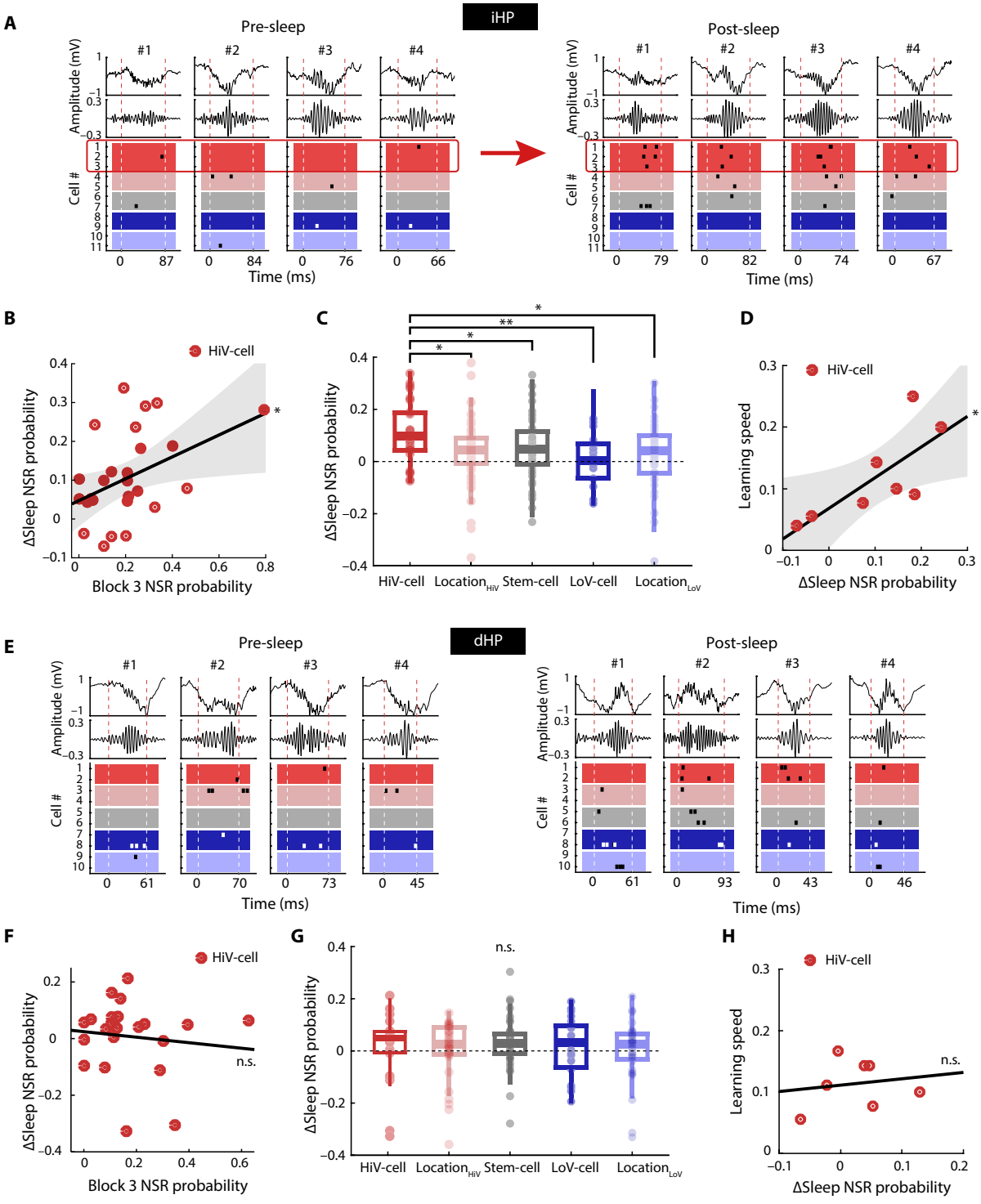

Fig. 7. Enhanced reactivation of HiV-cells in the iHP, but not in the dHP, is maintained during sleep after the place-preference task. (**A**) Illustrative examples of sleep SWR and reactivation activities that occurred during pre-sleep and post-sleep in the iHP. Raw LFP, 150- to 250-Hz filtered LFP, and NSR of cells #1 to 11 during the SWR period are shown. The cells used in (A) are the same as those in Fig. 4. The dashed line indicates the boundary of an SWR. (**B**) Scatter plot illustrating the correlation between NSR probability during the behavioral session and sleep by computing the degree of correlation between them. Each data point indicates the NSR probability of a single cell. The gray shaded indicates the 95% confidential interval of the linear regression. (**C**) Comparison of Δsleep NSR in the iHP among five types of place cells. Each data point denotes the NSR probability of a single cell ($N_{HiV} = 27$, $N_{LoV} = 26$, $N_{LocationHiV} = 46$, $N_{LocationLoV} = 45$, $N_{Stem} = 57$ cells). (**D**) Examination of the relationships between Δsleep NSR and learning speed on a subsequent day, based on the session mean NSR probability of HiV-cells in the iHP. Each data point represents the average NSR probabilities of HiV-cells per session. The gray shaded indicates the 95% confidential interval of the linear regression ($N = 8$ sessions). (**E** to **H**) The same analyses as in (A) to (D) were replicated in the dHP [(G) $N_{HiV} = 22$, $N_{LoV} = 23$, $N_{LocationHiV} = 32$, $N_{LocationLoV} = 32$, $N_{Stem} = 42$ cells; (H) $N = 7$ sessions]. See also figs. S4 and S5. *$P < 0.05$ and **$P < 0.01$.

along the dorsoventral (DV) axis of the hippocampus or is limited to the dorsal region of the hippocampus. Initially, we selected a route from a start location to a high-value location and visually represented this route with a color-coding scheme according to value (Fig. 8A). Population rate maps were constructed by combining place fields of ensemble cells from the dHP and iHP, respectively (Fig. 8B). Subsequently, using Bayesian decoding, we calculated the posterior probability for place cells that were recorded simultaneously during a SWR event (Fig. 8, C and D). In the dHP, place cells representing different places from the start location (indicated by blue data points in Fig. 8C) to the reward location (marked by red data points in Fig. 8C) were sequentially reactivated in either a forward direction (forward replay in #1 to 4 in Fig. 8C) or a reverse direction (reverse replay in #5 to 8 in Fig. 8C) within individual SWR events.

However, in the iHP, no such robust SRs were observed. Instead, place cells in the iHP seemed to collectively reactivate spatial representations near either the intersection of the T-maze (ripples #1 to 4 in Fig. 8D) or the choice arms (ripples #5 to 8 in Fig. 8D). Among the candidate SRs, we found 28 significant SRs in the dHP, but only one incident in the iHP (see Materials and Methods for details). The proportion of significant SR events among candidate replay in the dHP ($n = 28$ of 185; 15.1%) was significantly higher than that in the iHP ($n = 1$ of 71; 1.4%) ($P = 0.0019$; two-sample chi-square test) (Fig. 8E). Most SRs in the dHP ($n = 25$ of 28; 89.3%) represented the rat's navigational path leading to the high-value reward zone ($P < 0.01$; one-sample chi-square test) (Fig. 8F). This result aligns with previous literature on SR (*7*, *9*). Some may argue that the lack of SR in the iHP might be attributable to the idiosyncratic experimental conditions of the current study, such as insufficient allocentric cues or our behavioral protocols. However, this is unlikely because we observed robust SR in the dHP.

Differential spatial firing characteristics of place cells between the dHP and iHP

To further investigate the differential SR between the dHP and iHP, we examined whether place cells in the dHP and iHP represented the T-maze arms evenly or overrepresented the behaviorally significant locations. From the start to the choice point, both population rate maps recorded from the place cells in the dHP and iHP exhibited a similar accumulation of place fields near the choice point (Fig. 9A). From the choice point to the HiV-reward zone, place fields in the dHP had relatively linear representation along the choice arm. However, those in the iHP were aggregated near the reward location (Fig. 9A). To characterize these phenomena more quantitatively, we checked where the peak firing locations of cells were found by calculating the peak firing rate across spatial bins (bin size = 10 cm). The resulting histogram that ranged from the start to the choice point showed that place cells in both the iHP and dHP overrepresented the choice point ($P = 0.97$; two-sample Kolmogorov-Smirnov test) (Fig. 9B, left). In contrast, from the choice to the reward location, place fields in the dHP were evenly distributed, whereas those in the iHP were accumulated in the vicinity of the reward zone ($P < 0.05$; two-sample Kolmogorov-Smirnov test) (Fig. 9B, right). We also found that the place-field size and the size of field overlap between two place cells were significantly larger in the iHP than in the dHP ($P < 0.001$ for overlap index; $P < 0.001$ for field size; Wilcoxon rank-sum test; see details in Materials and Methods) (Fig. 9, C and D).

Next, we calculated how strongly cells could preserve their spatially sequential firing during SWRs. If the cells are activated following the same sequence as they fired during navigation from the start to the reward zone, then we consider it the most sequential firing order. We used the root mean square error (RMSE; see more details in Materials and Methods) to quantify the cell's sequential firing score (Fig. 9E). For example, if the firing sequence matches exactly the peak firing order of the population rate map (Fig. 8B), then RMSE value becomes 0, and it is considered the most sequential ordering. If the firing sequence during SWRs does not match the ordering of the peak firing location, then RMSE becomes larger. Although we found some sequentially firing cell assemblies in the iHP (#6 and #7 in Fig. 9F), we generally found stronger sequential firing patterns in the dHP than in the iHP (Fig. 9F). At the population level, RMSE was greater in the iHP than in the dHP ($P < 0.05$; Wilcoxon rank-sum test) (Fig. 9G), supporting our observations. We confirmed this result using the "match probability analysis" method previously used by Lee and Wilson (*20*) (fig. S6). Visualizing the relationships among RMSE, overlap index, and field size in 3D also corroborated our findings (Fig. 9H) (*20*). Collectively, our results suggest that place cells in the iHP tended to gather near the reward zone and have larger fields and overlap in addition to the weaker sequential firing order (Fig. 9H). These characteristics collectively contributed to the relative lack of SR in the iHP than in the dHP.

DISCUSSION

The current study investigated whether place cells in the iHP are reactivated differentially during SWR events after learning spatial value changes. We found that in the reward reversal block, HiV-cells in the iHP were reactivated more frequently than the remaining place cell types (LoV-cells, $\text{Location}_{\text{HiV}}$-cells, $\text{Location}_{\text{LoV}}$-cells, and stem-coding cells). Furthermore, the selective NSR of HiV-cells in the iHP was enhanced after rats learned the task after they acquired the reverse relationship between place and its associated reward value; moreover, the potentiated NSR of HiV-cells in the iHP was maintained in the post-sleep session. The frequent NSR of HiV-cells in the iHP during the post-sleep session facilitated place-value learning on the next day. However, such value-based, learning-dependent NSR was rarely observed in the dHP. Instead, we found that the spiking activities of place cells whose place fields were sequentially organized toward the high-value reward location were replayed more frequently in the dHP than in the iHP during SWRs. Overall, our findings suggest that functionally heterogeneous types of information are differentially and simultaneously reactivated in the dHP and iHP presumably to optimize goal-directed navigation for maximal reward.

Spiking activities representing high-value locations are selectively reactivated in the iHP but not in the dHP

In our experiments, we assumed that a subset of place cells that remapped their fields to represent high-value locations are specialized to encode the high value of a place. We found that HiV-cells in the iHP had higher NSR probabilities than the remaining cell types. These results suggest that the relative value of information associated with a place can modulate the NSR probabilities of place cells in the iHP. Although some prior studies have suggested that the function of the iHP is to encode and update the value of a place, to the

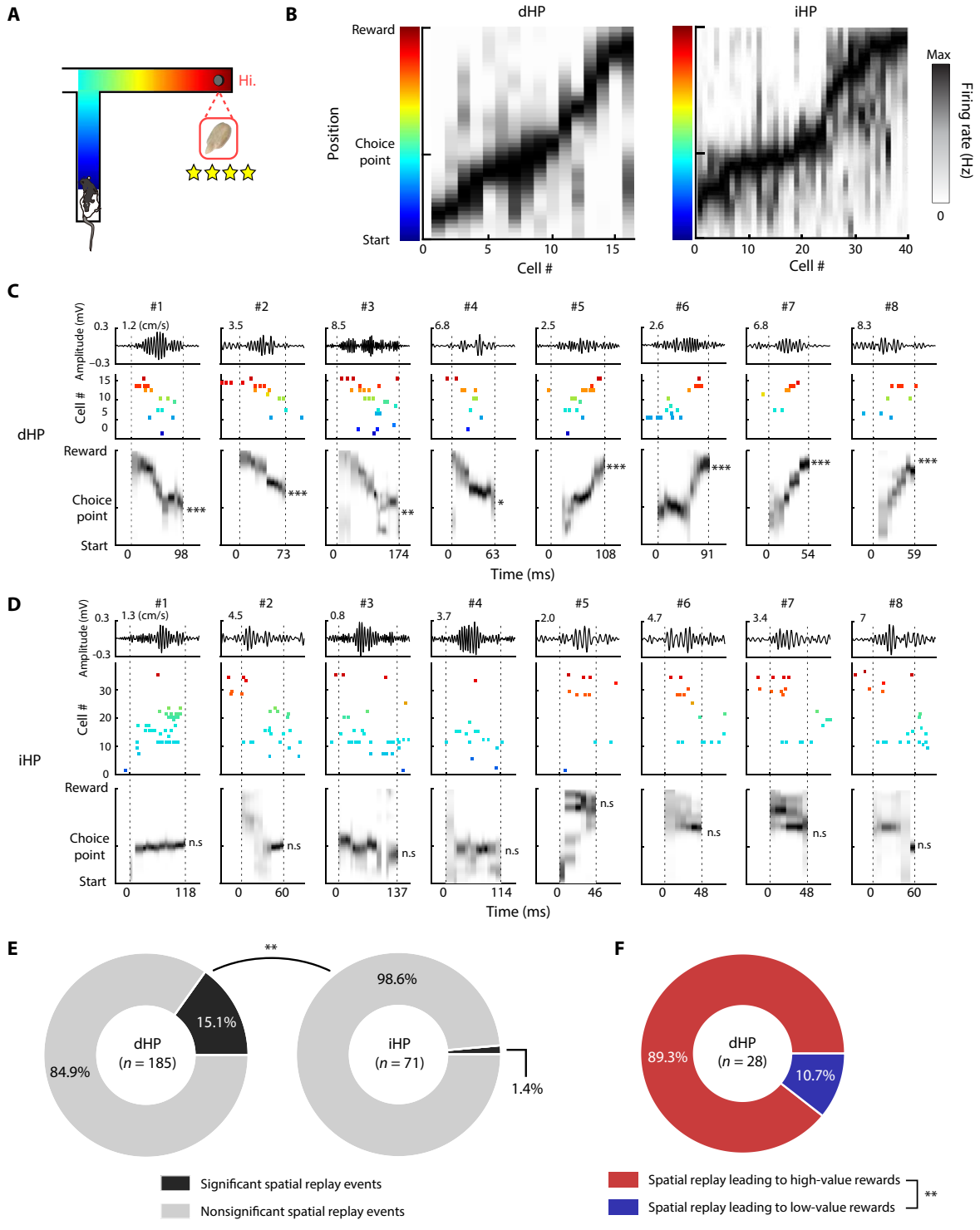

Fig. 8. Spatial replay leads toward the goal location in the dHP but not in the iHP. (**A**) T-maze illustration with color-coded positions. The color-coding map was used to visualize the SR examples presented in (C) and (D). (**B**) Population rate maps of ensemble place cells constructed from the dHP (left) and iHP (right). (**C** and **D**) Individual examples of SWRs and replay that occurred during occupation of the reward zone. Graphs of 150- to 250-Hz filtered LFP, color-coded reactivated spikes, and posterior probability of decoded position during an SWR are shown. The boundary of the SWR is indicated by a black dashed line; the calculated linear regression line is indicated by a red dashed line; and the statistical significance of permutation tests is denoted by an asterisk. The mean velocity (in centimeters per second) during an SWR is shown on the filtered LFP graph. (**E**) Pie chart showing the proportion of significant replay events between the dHP and iHP that occurred during occupation of the reward zone. The numbers of significant replays and candidate replay events are denoted in the bar (dHP: $N_{Sig.} = 28$ and $N_{Non\text{-}sig.} = 157$ cells; iHP: $N_{Sig.} = 1$ and $N_{Non\text{-}sig.} = 70$ cells). (**F**) The proportion of significant replays representing paths leading to either high-value or low-value reward zones ($N_{High} = 25$ and $N_{Low} = 3$ cells). $^{**}P < 0.01$.

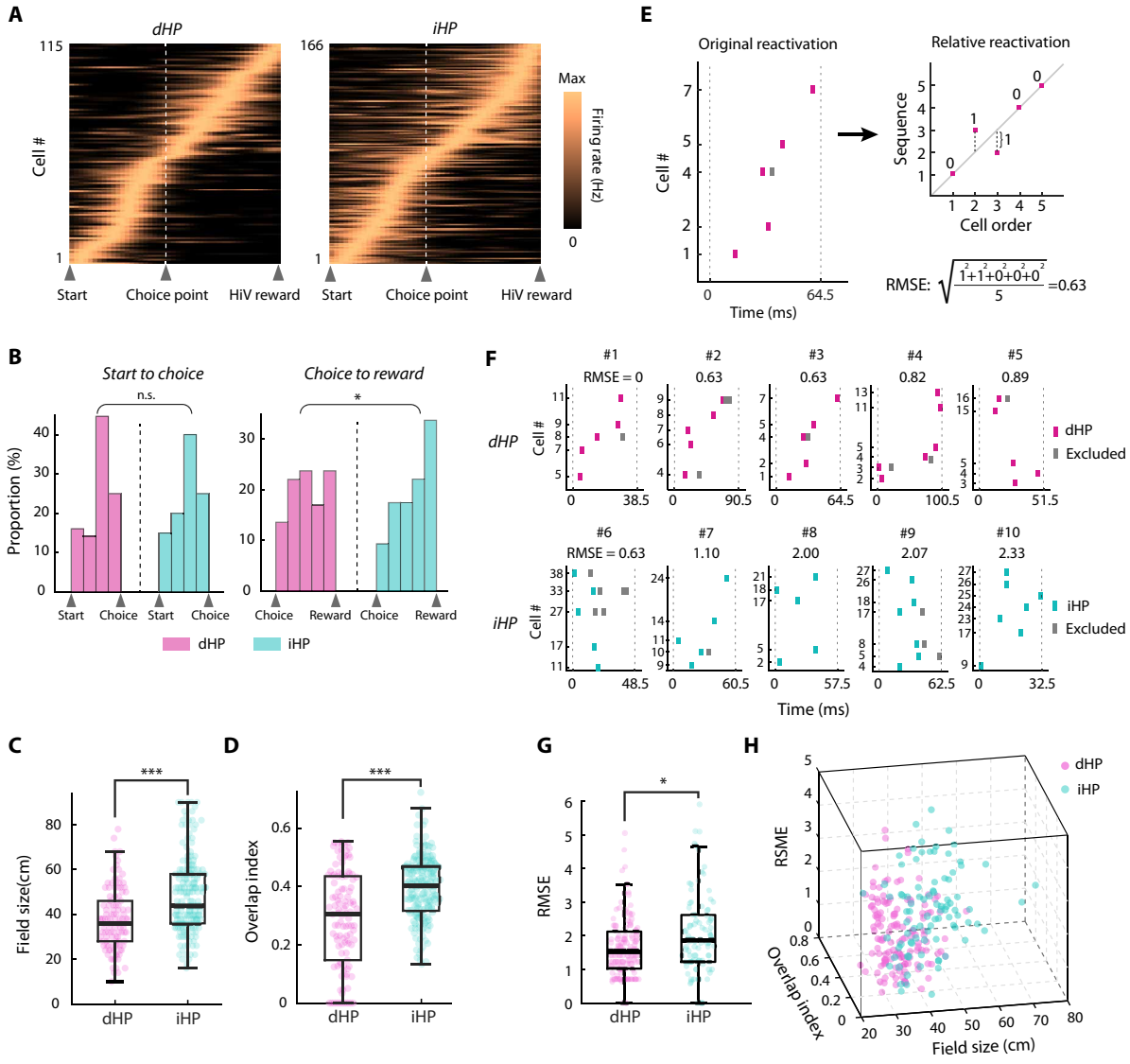

Fig. 9. Differential spatial firing characteristics of place cells between the dHP and iHP. (**A**) The population rate map that aligns the linearized place fields from the start to the reward location and is sorted by peak firing location, recorded from the dHP (left) and the iHP (right) (N_{iHP} = 115 and N_{dHP} = 166 cells). (**B**) Distribution of the proportion of bins whose peak firing is located within each bin. Position bins from the trial start to the choice point (left) and those from the choice point to the reward zone (right). (**C** and **D**) Boxplot comparing the field size (C) and overlap index (D) between dHP and iHP [(C) N_{iHP} = 115 and N_{dHP} = 166 cells, (D) N_{iHP} = 114 and N_{dHP} = 165 pairs]. (**E**) Illustration of the method of calculating sequential firing score using the root mean square error (RMSE). Spikes reactivated during SWRs (magenta ticks) are sorted by their peak firing location (Fig. 8B). Multiple spikes from the same cell within short inter-spike intervals are excluded (gray line). (**F**) Raw SWR examples to compare sequential firing patterns and their RMSE. The dotted line represents the start and the end of SWRs. Each tick represents the timing of spiking, where magenta represents dHP and cyan represents iHP. The gray bar represents excluded spikes. (**G**) Boxplot comparing RMSEs obtained from the dHP and iHP. (**H**) The 3D scatter plot of RMSE, overlap index, and field size. Each dot represents each SWR containing four or more place cells, and it is calculated by averaging the overlap score and field size of place cells that are active in each SWR [(G) and (H) N_{iHP} = 94 and N_{dHP} = 131 SWRs]. See also fig. S6. *$P < 0.05$ and ***$P < 0.001$.

best of our knowledge, the type or quality of information reactivated in the iHP has rarely been previously reported (*10*, *21*, *22*).

In our previous study (*10*), we found that place cells in the iHP exhibited more robust remapping in response to changes in reward value than those in the dHP, and their fields accumulated near high-value locations. Another study by De Saint Blanquat and colleagues (*22*) showed that inactivating the iHP by injection of muscimol impaired place-value updating in place-preference tasks, but no impairment was observed when the dHP was similarly inactivated. Furthermore, lesioning the iHP impaired the rapid learning of a place-learning task in which the location of the hidden escape platform changed daily (*21*) and abolished the goal-related activities of the medial prefrontal cortex in the place-preference task (*23*). These results imply that high-value–associated spatial information is reactivated selectively in the iHP and serves to facilitate associative learning between a place and its value.

In contrast, we found no such reactivation patterns in the dHP. Most studies of the dHP have focused on the reinstatement of

navigational trajectories (spatial replay) by sequential spatial firing (*24*–*28*). However, few studies have directly investigated whether the NSR patterns of cells are dependent on the relative values associated with different places in the dHP. It is worth noting that the results of some studies imply that reward information can modulate the SR or NSR probabilities of place cells in the dHP. For example, Ambrose and colleagues (*8*) showed that the frequency of reverse SR in the dHP was manipulated by the amount of reward provided in the reward zone in an experimental paradigm in which rats shuttled between two reward zones in a linear maze. Another study by Singer and Frank (*29*) argued that NSR probability was enhanced in the reward compared to the no-reward condition. These results are seemingly in conflict with other studies demonstrating that place cells in the dHP tend to exhibit value-insensitive firing when values associated with fixed reward locations change (*10*, *30*, *31*). This discrepancy may reflect the difference in behavioral tasks; in this case, rats were required to update spatial value from low (i.e., a small amount of reward) to a high value (i.e., a large amount of reward) in a goal-directed navigational task (*10*, *30*, *31*). In contrast, other studies used non-hippocampal-dependent tasks (*8*) or provided rewards only in one of two reward zones in a W-shaped maze (*29*).

Notably, some prior studies manipulated spatial value by associating an electric shock with a place (*32*). In this case, place fields in the dHP underwent global remapping after the animal experienced the electric shock. Our results are consistent with the idea that the spiking activities of place cells that remapped after associating a negative value with a certain place could also be reactivated more frequently than non-remapping cells. Ormond and colleagues (*33*) tested this idea using an aversive spatial decision-making task in which rats received an electric shock in the choice arm. After experiencing the shock, rats did not re-enter the shock-associated arm, and a subset of place cells in the dHP remapped their fields globally. NSR probabilities were higher in place cells that exhibited shock-related remapping in the dHP than in non-remapping cells. In another study, rats received an electric shock at the end of a linear track (*34*). After the shock experience, rats avoided the shock zone as they moved around on the track, and they found that SR toward the shock zone was observed more frequently than before the shock experience. These results suggest that a negative event at a particular location changes the value of the place and may alter the NSR probability of the cells representing the location or SR contents representing the navigational route, serving to strengthen the associative memory between the place and its value during SWRs.

Spatial replay leading to the high-value location is observed in the dHP but not in the iHP

Previous studies reported that spatial paths leading to goal locations are sequentially replayed more in the dHP than those leading to non-goal locations (*7*, *9*, *26*). On the basis of our prior study showing that place cells in the iHP overrepresent high-value locations compared with low-value locations (*10*), we originally expected SRs leading to goal locations to occur more frequently in the iHP than the dHP. However, SR leading to high- and low-value locations was barely detectable in the iHP. Instead, we found robust SRs in the dHP, as has been frequently reported (*6*, *19*, *35*). The iHP may not be an ideal region for the occurrence of such SRs of precise location information because the size of the place field is larger and spatial tuning is poorer in the iHP compared with the dHP (*10*, *36*, *37*), and sequential firing is weaker in the iHP than in the dHP (Fig. 9). Instead, the larger place fields in the iHP may make the area suitable for representing spatial values, given that the spatial resolution of value is expected to be lower than that of a place in a natural environment.

In the current study, 85% of SR events in the dHP represented sequential paths to the higher-value location, whereas only 15% of SR events represented paths to the low-value location. Thus, the direction of SR in the dHP seems biased toward the high-value location, which aligns well with prior studies (*7*, *9*, *26*). For example, using a dual-environment reward-place association task on an eight-arm maze, Michon and colleagues (*9*) found that hippocampal SR events are biased toward paths associated with high-value (i.e., large reward) locations compared with those associated with low-value reward locations. Other studies reported that when rats learned the location associated with reward in an open arena, trajectories leading to that location were replayed more frequently than those leading to no-reward locations (*7*, *26*). The reported results of the SR in the dHP preferentially representing the trajectories to the high-value arm indicate that, if there are significant SRs of place cells, then their reconstructed paths will most likely be directed toward the high-value reward. However, during SWRs with fewer than four active place cells or during nonsignificant SRs, we found that place cells in the dHP encoding low-value arms were similarly engaged in NSR during the correct trials. This phenomenon could be linked to the simulation of visiting low-value zones or recalling recent low-value visiting experiences (*38*).

In addition, SRs could be directed to non-goal locations where animals underwent fearful events or where they received the satiated type of reward. Specifically, Wu and colleagues (*34*) identified an imaginary SR leading to the place where rats underwent an electric shock at the end of the linear track, even though rats did not enter the shock zone. Carey and colleagues (*39*) used different motivational states (i.e., thirsty or hungry) to bias the rat's navigation toward the choice arm containing the deprived reward (i.e., water or food) in the T-maze. They reported that SR occurred in the opposite direction relative to where the restricted reward was located, although rats shifted their behavior toward the restricted reward location. These results collectively suggest that the SR of place cells in the dHP is modulated by spatial value information when different places are associated with positive or negative values in the environment.

Reactivation of place cells in the iHP coding high spatial values is potentiated by subsequent sleep

It is well known that neural firing patterns acquired during a recent experience are reactivated in the hippocampus during subsequent sleep. For example, two place cells whose fields overlap in an open arena exhibit an increased tendency to be reactivated together during the following sleep session (*4*). Also, the firing sequence of place cells during active behavior is observed again during reactivation in the post-sleep session (*20*). In the current study, we found that place cells coding high spatial values in the place-preference task had higher NSR probabilities during SWRs, and they sustained their potentiated NSR during subsequent post-sleep sessions. The more frequent reactivation of motivationally salient information during sleep may facilitate the selective consolidation of such memories from the hippocampus to neocortical networks. Consistent with this idea, we found a positive correlation between the amount of sleep NSR of HiV-cells in the iHP and learning speed the next day.

These results imply that higher-value spatial events are reactivated more during post-behavioral sleep, presumably for their high priority during consolidation, and that learning on the next day may depend on such selective consolidation.

If information about high-value locations was consolidated during a post-sleep session on day 1, then one might think that rats also learned the high-value location quickly in block 2 the next day. However, we found that the number of trials to reach the learning criterion (performance >75%) in block 2 had large variability until day 2. Rats showed stable and rapid learning in block 2 from day 3 (fig. S1H). This disparity might be explained by the fact that there are two types of learning going on in the place-preference task. One is to learn the high-value location, and the other is to learn that they need to use an allocentric navigational strategy. Although rats learned the high-value location within one session, it took more than 1 day to learn that they had to use the spatial strategy during block 2. On the basis of the rats' learning curve across days 1 to 4, it became evident that the rats exhibited consistent and rapid learning from day 3. The results suggest that rats completed learning of the allocentric navigational rule on day 3.

MATERIALS AND METHODS

Subjects

Six male Long-Evans rats (RRID: RGD_18337282) weighing 300 to 400 g were used. Food was restricted to maintain body weight at 85% of free-feeding weight to sustain a higher motivation level in behavioral tasks; water was available ad libitum. Animals were housed individually under a 12-hour light/dark cycle. All protocols and procedures conformed to the guidelines of the Institutional Animal Care and Use Committee of Seoul National University (SNU-230427-1-2).

Behavior paradigm

Place-preference task (T-maze)

An eight-arm maze (central platform size, 401 cm^2; arm size, 8 × 45 cm; height, 70 cm from the floor) was converted to a T-maze by installing a T-shaped transparent acrylic structure in the center platform. The rat was confined to the start arm by an acrylic blocker. A food well (2 cm in diameter and 8 mm in depth) was located at the end of each arm, with a proximity sensor installed underneath the well to detect the displacement of an acrylic disc (2.5 cm in diameter) that covered the food well. An infrared sensor was installed at each arm entry. Transistor-transistor logic sensor signals were transmitted to a data-acquisition system (Digital Lynx SX, NeuraLynx). A light-emitting diode (LED)–light complex to illuminate the experimental room and digital cameras to monitor animals' positions were installed on the ceiling. The maze was surrounded by circular black curtains to which a considerable number of visual cues were attached. White noise (80 dB) was delivered through two loudspeakers during the recording session to mask unwanted noise in the environment. In the place-preference task, rats were required to choose an arm baited with a more preferred type of reward [i.e., SS or whole SS ($^4/_4$ SS)] over a less-preferred reward [i.e., Cheerios cereal (CR) or quarter SS ($^1/_4$ SS)]. Rats initially learned the arm in which the more preferred reward was baited by trial and error in block 1. In block 2, rats were started from the opposite start arm to make the task more hippocampal-dependent (*13*). In block 3, they started from the original starting arm but the locations associated with higher-value and lower-value rewards were reversed. This experimental design sought to examine the rat's behavior and neural correlates when updating place and its associated value in the environment (Fig. 1A). Each block was terminated when rats chose the arm baited with the preferred reward more than 12 times in the previous 15 trials. After the rats had been tested for 2 days with SS and CR rewards, they were tested in the same task, but this time, they were provided the preferred type of reward (SS) only in the two reward arms but in different amounts (i.e., $^4/_4$ SS versus $^1/_4$ SS). The higher-value location on the first day was pseudo-randomly determined, and all rats departed from the south arm in block 1. The location of the high-value location the next day was the same as that of the last high-value location the day before.

Maze pre-training and surgery

After rats had become familiarized with the maze environment for a few days (30 min/day), they were trained in a shuttling task in which they alternated between the two adjacent arms of the eight-arm maze to obtain rewards. Rats were trained to complete 240 trials in 1 hour, which took approximately 4 days (mean, 3.8 days; SD, 1.1 days). After pre-training, a hyperdrive containing 24 tetrodes was implanted for recording spikes from single units and LFPs. Tetrodes were made using platinum wires (17.8 μm in diameter). A semiautomatic plating device (nanoZ, NeuraLynx) was used to adjust the final impedance of each tetrode to approximately 130 kilohms (measured in gold solution at 1 kHz). The hyperdrive was configured to have two separate electrode bundles, one carrying 18 tetrodes to target across the longitudinal axis of the hippocampus, and our coordinates were designed to mostly target the iHP but not the ventral hippocampus (vHP; coordinates for implantation: 5 mm posterior to bregma, 6 mm lateral from midline), and the other containing six tetrodes to target the dHP (coordinates for implantation: 3.2 mm posterior to bregma, 3 mm lateral from midline). Although a few tetrodes landed in the vHP, we excluded the data collected from the single units recorded from the vHP mainly because of the lack of "place cells" in the vHP. That is, the main objective of the study was to investigate the neural activities of place cells representing higher-value locations compared to the lower-value locations, but the lack of place cells makes the vHP not analyzable. The bundles were inserted obliquely (5° medially from the vertical axis) into the hyperdrive frame so that the tetrodes could maximally target the cell layers in the iHP.

Post-surgical training and main recordings

After 1 week of recovery from surgery, rats were retrained in the shuttling task. Retraining of rats to the same presurgical criterion required 10 ± 3 days (means ± SD). During the post-training period, tetrodes were gradually lowered into the CA1 cell layer in the hippocampus, while the rat was at rest on a pedestal. Once most tetrodes reached their target cell layers in the dorsal and intermediate-ventral regions in the hippocampus, the main recordings began. Place cell activity was recorded, while rats shuttled on the two adjacent arms (spatial alternation task) for 7 days according to a previously detailed experimental protocol (*10*). On days 8 to 11, rats performed the place-preference task in the T-maze. SS and CR were used as high-value and low-value rewards for recording on days 8 and 9, respectively, and $^4/_4$ SS (high value) and $^1/_4$ SS (low value) were used for days 10 and 11, respectively. One session consisted of blocks 1 to 3, and rats performed one session per day. Thus, we

recorded a total of 24 sessions from six rats. Because of the low signal-to-noise ratio of the ripple band in seven sessions and failure in reward reversal learning in block 3 in two sessions, we used a total of 15 sessions from five rats in the main analysis. Sleep sessions were recorded for approximately 30 min before and after the place-preference task while rats were at rest or asleep.

Electrophysiological recording procedures

After 1 week of recovery, each rat was placed on a custom-built pedestal outside the experimental room and habituated to rest for tetrode adjustment. Tetrodes were lowered individually to the cell layers over ~2 weeks. Neural activity was amplified (1000 to 10,000 times) and digitized (sampling frequency, 32 kHz; filtered at 600 to 6000 Hz for spiking data and 0.1 to 1000 Hz for LFP) using a Digital Lynx system (NeuraLynx). The rat's position and head direction were measured using an array of red and green LEDs attached to a custom headstage complex coupled to a preamplifier (HS-36; NeuraLynx). A ceiling camera recorded LED positions and fed the signal to a frame grabber (sampling frequency, 30 Hz).

Histological verification of electrode tracks

After completion of the main recording sessions, tetrode-tip locations were marked by passing a weak electrical current through each tetrode (10 μA for 10 s). On the next day, the rat was euthanized using an overdose of carbon dioxide (CO_2) and then was perfused transcardially, first with phosphate-buffered saline and then with a 4% (v/v) formaldehyde solution. Thereafter, the brain was removed and kept in a 4% v/v formaldehyde containing 30% sucrose solution at 4°C until it sank. The brain was sectioned in the coronal plane at 40-μm thickness using a sliding microtome (HM 430, Thermo Fisher Scientific), mounted on a sliding glass, and then stained with thionin. Photomicrographs were taken using a digital camera attached to a microscope (Eclipse 80i, Nikon). Tetrode tracks were reconstructed using a series of sections, taking into account the presurgical configuration of the tetrode-array bundle and electrolytic lesion marks. DV recording positions of place cells were quantitatively measured as the vertical distance from the cortical surface to electrode tip locations.

Data analysis

Unit isolation

Spikes associated with single units were isolated using a Windows-based, custom-written program (WinClust). The parameters, peak, valley, energy, and spike width, calculated from waveforms recorded from the four channels of a tetrode, were used for isolation. Unit isolation quality was evaluated during cluster-cutting procedures, with each cluster defined as isolation quality 1 (poorly isolated) to 5 (well isolated) based on how well the cluster was separated from neighboring clusters and background noise. Units with an isolation rating of 1 were excluded from further analysis. Inter-spike interval (ISI) histograms were also used to judge the quality of the cut cluster. Units showing a mean firing rate >10 Hz (either in the open field or in the radial maze) with a spike width <300 μs were classified as inhibitory interneurons and were excluded from further analysis.

Sharp-wave ripple detection

SWRs were extracted from LFPs using the following steps. First, the two tetrodes that recorded the largest SWRs were selected, and the corresponding LFP signals were filtered with a 150- to 250-Hz bandpass filter. Sections exceeding four SDs from the average of the filtered signals were initially selected, and the point where enhanced signals decreased by less than 1 SD was taken as the boundary of the SWR for each tetrode. The SWR boundary was determined as the sum of the SWR boundaries of two tetrodes. If only one tetrode exceeded the threshold within a particular section, then it was not counted as an SWR. Next, the number of cells reactivated within the SWR boundary was measured. If the number of reactivated cells was less than 5% of the total number of recorded cells, then the signal was considered noise. Last, signals recorded during the passage of an SWR boundary were also considered noise if the animal's head movement speed at the time was >20 cm/s (e.g., bumping noise due to collision with the acrylic blocker installed in the T-maze). For spectrogram analysis, we selected the tetrode that exhibited maximal SWR amplitude in the dHP and iHP, respectively. We used the built-in MATLAB function 'mtspecgramc' from Chronux 2.12 to calculate the spectrogram. The detailed parameters used were as follows: 'fpass = [50 350],' 'tapers = [3 5],' 'trialave = 1,' and 'moving window = 100 ms with 10-ms increments within a window ranging from −200 ms to +200 ms.'

Local and global SWRs

If SWRs were only detected in either the dHP or iHP, they were classified as a local ripple. Global ripples were further classified by (i) 'synchronized,' (ii) 'dHP-leading,' and (iii) 'iHP-leading.' This is determined by the difference in the time points of ripple peaks (ΔTime; dHP - iHP) between the dHP and iHP. If ΔTime is within −10 to 10 ms, then it is considered 'synchronized.' If ΔTime is smaller than −10 ms, then it is considered 'dHP-leading.' If ΔTime is greater than 10 ms, then it is considered 'iHP-leading.' When targeting the dHP and iHP using our surgical coordinates, the distance between the dHP and iHP was greater than 3.5 mm (fig. S1, A and B). Thus, we set 10 ms as a threshold using the minimum distance between the two regions and considering the estimated ripple propagation velocity (0.35 mm/1 ms) (*16*). To calculate the chance level of ΔTime distribution, we randomly shifted (between −5 and 5 s) each ripple peak time and calculated the distribution 10,000 times. The black dotted line represented the upper 95% of the shuffled distribution (fig. S2G).

Basic firing properties

To construct a rate map, we first scaled the 720 × 480 pixel space down to 72 × 48 pixel space (1 pixel = 2 × 2 cm). The firing rate associated with a given pixel was calculated by dividing the number of spikes by the time spent in each pixel (i.e., spike per second in each pixel). The raw rate map was then smoothed using an adaptive binning method. The amount of spatial information associated with a single spike of a single unit was measured by calculating spatial information based on the firing rate map, according to the following equation (*40*)

$$\text{Spatial information} = \sum p_i \frac{\lambda_i}{\lambda} \log_2 \frac{\lambda_i}{\lambda} \left(\frac{\text{bit}}{\text{spike}} \right)$$

where i denotes bin, p_i is the occupancy rate in the ith bin, λ_i indicates the mean firing rate in the ith bin, and λ is the overall mean firing rate. Stability within the square box test was measured by comparing the firing rate map between the first half and the second half of the session using Pearson's correlation.

Behavior analysis

For learning curve analyses, we calculated the estimated learning curve and the trial at which the rat reaches acquisition onset by applying a state-space model to behavioral performance (*14*). Latency is the time elapsed from passing by the infrared sensor installed at

the entry of the start arm to reaching the food well. Learning speed is the inverse value of the trials to reach the learning criterion. In Fig. 7 (D and H), we measured the learning speed in block 1 on the next day. Because the high-value location of the first block on the day of the experiment was the same as the last block on the previous day, faster learning by rats in the first block was taken to mean that the information of high-value locations was strongly strengthened by sleep reactivation of high–value-coding place cells in the iHP.

Place cell analysis

A place cell was defined by applying the following steps. First, the spatial rate map, smoothed using Skaggs's adaptive binning method, was calculated, and the pixel with the maximal firing rate was identified. Then, the firing rates associated with all other pixels were compared against the maximal firing rate, and only those pixels whose firing rate exceeded 20% of the peak firing rate were retained for further analysis. Among the remaining pixels, one or more sets of continuous pixels (>40 cm^2 in size with a peak firing rate >1 Hz) were defined as place fields. In cases where multiple place fields were found during the procedure, the field size of the unit was calculated by taking the sum of all subfields as the unit's field size. Spiking data were included only if instantaneous speeds were greater than 5 cm/s at the time of the spike; spikes in the reward zones were excluded from the analysis (*41*). Because a proximity sensor was installed inside the food well, the exact timestamp when rats displaced the disc covering the reward could be measured. A cell was operationally defined as a place cell if (i) its field size was greater than 40 cm^2, and its peak and mean firing rates were greater than 1 and 0.25 Hz, respectively; and (iii) its spatial information was higher than 0.25 bits per spike with a statistical significance of $P < 0.01$ (*40*, *42*).

The degree of changes in firing rate maps in response to the reversal of reward contingency was measured by Pearson's correlation coefficients between rate maps before (i.e., block 1) and after the reward reversal (i.e., block 3). If correlation coefficients were greater than 0.75, then we defined this cell has stable rate maps regardless of reward reversal (i.e., location-coding place cells). If these were lower than 0.75, then we considered these had global remapping (value-coding place cells). By using only post-learning trials of block 3, we constructed post-learning spatial rate maps, and these were used to dissociate place cells into five cell types (i.e., HiV-cells, $Location_{HiV}$-cells, and LoV-cells, $Location_{LoV}$-cells, and stem-coding cells) (Fig. 3). HiV-cells and LoV-cells were subdivided into (i) Turn-on cells where place cells were silent in block 1 (i.e., before reward reversal), but place fields appeared on either HiV-arm or LoV-arm in block 3 (i.e., after reward reversal) and (ii) Shift cells where firing fields shifted from one reward location or stem in block 1 to either HiV-arm or LoV-arm in block 3 to encode the value of an arm.

The place cell's overlap index is calculated as the intersection over the union of the two place cells. It ranges from 0 to 1, and if the index is 1, two place fields are completely overlapped. For Fig. 9D, we computed the overlap index based on the population rate map in Fig. 9A. In Fig. 9H, we calculated the overlap index and field size per each ripple by averaging the active place cell's overlap index and field size per SWRs.

Nonspatial reactivation analysis

We calculated NSR probability and reactivation rate to measure how many times a single-place cell was activated during the SWR epoch. Specifically, NSR probability was calculated by dividing the number of SWRs in which one place cell was reactivated by the total number of SWRs. The reactivation rate was measured by dividing the number of total reactivated spikes by the sum of total SWR durations. The same calculations were applied to pre- and post-sleep sessions, and the entire (~30 min) pre- and post-sleep dataset was used for calculating reactivation activities.

Constructing the population rate map

Population rate maps for the place-preference task were constructed by linearizing spatial rate maps for all place cells and stacking them (bin size = 2 cm). Trials in the post-learning stages of block 3 were used to create a population rate map (Fig. 3, B and D). The firing rate in each bin was calculated by dividing the number of spikes by the number of occupancies by the rat within that bin. In the curved section, a fan-shaped boundary with an internal angle of 22.5° was defined as a bin. Linearized firing rate maps were smoothed using a Gaussian window (window size, 22 cm; full width at half maximum, 10 cm).

Bayesian decoding for position reconstruction

The rat's positional information was reconstructed from the activity of place cells by applying a Bayesian decoding algorithm (*43*, *44*). In Bayesian analysis, value-coding place cells, location-coding place cells, and place cells whose fields were in the stem of the T-maze were pooled. Briefly, the number of spikes at a given time t, $n_i(t)$, was calculated for each place cell, i. The 2D spatial rate map was linearized to a 1D spatial rate map, and the mean firing rate at a given spatial position x, $\lambda_i(x)$, was calculated. The reconstruction was obtained using two vectors, $n(t) = (n_1, n_2, \ldots n_N)$ and $\lambda(x) = (\lambda_1, \lambda_2, \ldots \lambda_N)$, where "$N$" is the number of recorded place cells, and the firing probability was assumed to follow a Poisson distribution.

The animal's position was reconstructed using the standard formula for conditional probability (1)

$$P(x/n)P(n) = P(n/x)P(x) \tag{1}$$

where $P(x)$ is the probability that the animal is positioned at x, and $P(x/n)$ is the conditional probability that the animal is located at position x when the spike count was n. This equation Equation 1 is rearranged to Eq. 2 to solve for the conditional probability of the reconstructed animal's position

$$P(x/n) = \frac{P(n/x)P(x)}{P(n)} \tag{2}$$

Assuming that the firing characteristics of each place cells follow a Poisson distribution and that all cells fire independently, the prior template, $P(n/x)$, was calculated as Eq. 3

$$P(n/x) = \prod_{i=1}^{N} P(n_i/x) = \prod_{i=1}^{N} \frac{\left[\tau\lambda_i(x)\right]^{n_i}}{n_i!} \exp\left[-\tau\lambda_i(x)\right] \tag{3}$$

where τ is the time window for data sampling (20 ms). Thus, $P(x/n)$ was calculated according to Eq. 4

$$P(x/n) = \frac{\prod_{i=1}^{N} \left\{ \frac{\left[\tau\lambda_i(x)\right]^{n_i}}{n_i!} \right\} \exp\left[-\tau \sum_{i=1}^{N} \lambda_i(x) \right] P(x)}{P(n)} \tag{4}$$

and $P(n)$ was used to normalize probabilities (*43*). The position at which $P(x/n)$ was maximum was the reconstructed position ($\hat{x}$)

$$\hat{x} = \text{argmax} P(x/n)$$

Spatial replay events

A candidate SR event consisted of four or more place cells participating in each SWR event ($n = 185$ for dHP, $n = 71$ for iHP). If less than four place cells were activated in each SWR event, then we excluded it from the SR analysis, but it was still included in the NSR analysis. For each candidate SR event, we calculated the posterior probability using Bayesian decoding, followed by a linear regression to calculate the coefficient of determination (r^2). We shuffled the rate maps by circularly shifting linearized rate maps, then computed shuffled r^2 and repeated it 1000 times. In addition, we computed replay length by subtracting the maximum posterior probability location of the first-time bin from that of the last-time bin. If the actual r^2 value was in the upper 95% of the shuffled r^2 distribution (i.e., $P < 0.05$) and the replay length was greater than 30 cm, then an event was considered a significant SR event.

Match probability analysis

Match probability analysis is used to compute the strength of sequential firing order, which was developed by Lee and Wilson (*20*). We used the same method described in this paper. In short, this method finds the best matching word generated by reactivation spikes in each RUN sequence and then calculates the probability that the word will include such a match or a better match under the assumption that all possible permutations of constituent characters are equally likely. For example, in the RUN sequence 123456789ABCDEF, the word 57AFC has the best match (4,0) and there is a better match (5,0). The probability (p) of obtaining a matching item beyond this is $(1 + 8)/5! = 0.075$ (fig. S6A). Then, we calculated the z-score to normalize how sequentially it is far from the $P = 1/4$!

Root mean square error (RMSE)

The RMSE value was used to quantify spiking's sequential firing order during SWRs. First, the relative firing order of the spikes was determined on the basis of the order of the reactivated spikes in reactivation. Based on Lee and Wilson (*20*), we only used the first spike of spike trains with the hypothesis that the first spike contains the most important information. However, spikes with a sufficiently large ISI (>100 ms) were treated as distinct order sets. We computed all values representing the deviation of the relative order from the original sequence. This procedure was calculated for both scenarios, forward and reverse replay, and we took a smaller RMSE value for our analysis. For example, in the case of reactivation shown as an example in Fig. 9E, the relative order is 1-3-2-4-5, and because the second and third spikes are in the original order of 3 and 2, respectively, each square of error in the figure is calculated as $(2-3)^2$ and $(3-2)^2$. Thus, the forward RMSE value is calculated as $\sqrt{\left[(0+1+1+0+0)/5\right]} = 0.63$. Similarly, the reverse RMSE value is 2.76. In addition, we chose 0.63 as its RMSE value.

Statistical analysis

Statistical testing was performed with MATLAB using built-in and custom-made functions. The null hypothesis was rejected using the nonparametric Wilcoxon rank sum and Kruskal-Wallis tests. A chi-square test was used to test the proportional difference between groups. The significance of linear relationships between two dependent variables was tested using linear regression. We used a two-sample Kolmogorov-Smirnov test to examine whether the distributions of the two groups significantly differed. A Bonferroni correction was used to correct the significance level. Statistical results are reported in the Results sections. All tests were two-tailed, and significance was accepted at a P value of 0.05.

Supplementary Materials

This PDF file includes:

Figs. S1 to S6
Legend for movie S1
Legend for data file S1

Other Supplementary Material for this manuscript includes the following:

Movie S1
Data file S1

REFERENCES AND NOTES

1. H. Eichenbaum, A cortical-hippocampal system for declarative memory. *Nat. Rev. Neurosci.* **1**, 41–50 (2000).
2. H. Eichenbaum, N. J. Cohen, *From Conditioning to Conscious Recollection: Memory Systems of the Brain* (Oxford Univ. Press, 2001).
3. L. R. Squire, C. E. Stark, R. E. Clark, The medial temporal lobe. *Annu. Rev. Neurosci.* **27**, 279–306 (2004).
4. M. A. Wilson, B. L. McNaughton, Reactivation of hippocampal ensemble memories during sleep. *Science* **265**, 676–679 (1994).
5. G. Buzsaki, Two-stage model of memory trace formation: A role for "noisy" brain states. *Neuroscience* **31**, 551–570 (1989).
6. D. J. Foster, M. A. Wilson, Reverse replay of behavioural sequences in hippocampal place cells during the awake state. *Nature* **440**, 680–683 (2006).
7. B. E. Pfeiffer, D. J. Foster, Hippocampal place-cell sequences depict future paths to remembered goals. *Nature* **497**, 74–79 (2013).
8. R. E. Ambrose, B. E. Pfeiffer, D. J. Foster, Reverse replay of hippocampal place cells is uniquely modulated by changing reward. *Neuron* **91**, 1124–1136 (2016).
9. F. Michon, J. J. Sun, C. Y. Kim, D. Ciliberti, F. Kloosterman, Post-learning hippocampal replay selectively reinforces spatial memory for highly rewarded locations. *Curr. Biol.* **29**, 1436–1444.e5 (2019).
10. S. W. Jin, I. Lee, Differential encoding of place value between the dorsal and intermediate hippocampus. *Curr. Biol.* **31**, 3053–3072.e5 (2021).
11. J. L. Gauthier, D. W. Tank, A dedicated population for reward coding in the hippocampus. *Neuron* **99**, 179–193.e7 (2018).
12. P. Jarzebowski, Y. A. Hay, B. F. Grewe, O. Paulsen, Different encoding of reward location in dorsal and intermediate hippocampus. *Curr. Biol.* **32**, 834–841.e5 (2022).
13. M. G. Packard, J. L. McGaugh, Inactivation of hippocampus or caudate nucleus with lidocaine differentially affects expression of place and response learning. *Neurobiol. Learn. Mem.* **65**, 65–72 (1996).
14. A. C. Smith, L. M. Frank, S. Wirth, M. Yanike, D. Hu, Y. Kubota, A. M. Graybiel, W. A. Suzuki, E. N. Brown, Dynamic analysis of learning in behavioral experiments. *J. Neurosci.* **24**, 447–461 (2004).
15. H. Jeong, V. M. K. Namboodiri, M. W. Jung, M. L. Andermann, Sensory cortical ensembles exhibit differential coupling to ripples in distinct hippocampal subregions. *Curr. Biol.* **33**, 5185–5198.e4 (2023).
16. J. Patel, E. W. Schomburg, A. Berenyi, S. Fujisawa, G. Buzsaki, Local generation and propagation of ripples along the septotemporal axis of the hippocampus. *J. Neurosci.* **33**, 17029–17041 (2013).
17. J. Ferbinteanu, M. L. Shapiro, Prospective and retrospective memory coding in the hippocampus. *Neuron* **40**, 1227–1239 (2003).
18. L. M. Frank, E. N. Brown, M. Wilson, Trajectory encoding in the hippocampus and entorhinal cortex. *Neuron* **27**, 169–178 (2000).
19. K. Diba, G. Buzsaki, Forward and reverse hippocampal place-cell sequences during ripples. *Nat. Neurosci.* **10**, 1241–1242 (2007).
20. A. K. Lee, M. A. Wilson, Memory of sequential experience in the hippocampus during slow wave sleep. *Neuron* **36**, 1183–1194 (2002).
21. T. Bast, I. A. Wilson, M. P. Witter, R. G. Morris, From rapid place learning to behavioral performance: A key role for the intermediate hippocampus. *PLoS Biol.* **7**, e1000089 (2009).
22. P. D. S. Blanquat, V. Hok, E. Save, B. Poucet, F. A. Chaillan, Differential role of the dorsal hippocampus, ventro-intermediate hippocampus, and medial prefrontal cortex in updating the value of a spatial goal. *Hippocampus* **23**, 342–351 (2013).
23. B. G. Burton, V. Hok, E. Save, B. Poucet, Lesion of the ventral and intermediate hippocampus abolishes anticipatory activity in the medial prefrontal cortex of the rat. *Behav. Brain Res.* **199**, 222–234 (2009).
24. J. Widloski, D. J. Foster, Flexible rerouting of hippocampal replay sequences around changing barriers in the absence of global place field remapping. *Neuron* **110**, 1547–1558.e8 (2022).

25. X. Mou, A. Pokhrel, P. Suresh, D. Ji, Observational learning promotes hippocampal remote awake replay toward future reward locations. *Neuron* **110**, 891–902.e7 (2022).
26. H. Igata, Y. Ikegaya, T. Sasaki, Prioritized experience replays on a hippocampal predictive map for learning. *Proc. Natl. Acad. Sci. U.S.A.* **118**, e2011266118 (2021).
27. A. K. Gillespie, D. A. Astudillo Maya, E. L. Denovellis, D. F. Liu, D. B. Kastner, M. E. Coulter, D. K. Roumis, U. T. Eden, L. M. Frank, Hippocampal replay reflects specific past experiences rather than a plan for subsequent choice. *Neuron* **109**, 3149–3163.e6 (2021).
28. B. Bhattarai, J. W. Lee, M. W. Jung, Distinct effects of reward and navigation history on hippocampal forward and reverse replays. *Proc. Natl. Acad. Sci. U.S.A.* **117**, 689–697 (2020).
29. A. C. Singer, L. M. Frank, Rewarded outcomes enhance reactivation of experience in the hippocampus. *Neuron* **64**, 910–921 (2009).
30. E. Duvelle, R. M. Grieves, V. Hok, B. Poucet, A. Arleo, K. Jeffery, E. Save, Insensitivity of place cells to the value of spatial goals in a two-choice flexible navigation *task*. *Neuroscience* **39**, 1578–1518 (2019).
31. E. Tabuchi, A. B. Mulder, S. I. Wiener, Reward value invariant place responses and reward site associated activity in hippocampal neurons of behaving rats. *Hippocampus* **13**, 117–132 (2003).
32. M. A. Moita, S. Rosis, Y. Zhou, J. E. LeDoux, H. T. Blair, Putting fear in its place: Remapping of hippocampal place cells during fear conditioning. *J. Neurosci.* **24**, 7015–7023 (2004).
33. J. Ormond, S. A. Serka, J. P. Johansen, Enhanced reactivation of remapping place cells during aversive learning. *J. Neurosci.* **43**, 2153–2167 (2023).
34. C. T. Wu, D. Haggerty, C. Kemere, D. Ji, Hippocampal awake replay in fear memory retrieval. *Nat. Neurosci.* **20**, 571–580 (2017).
35. M. P. Karlsson, L. M. Frank, Awake replay of remote experiences in the hippocampus. *Nat. Neurosci.* **12**, 913–918 (2009).
36. K. B. Kjelstrup, T. Solstad, V. H. Brun, T. Hafting, S. Leutgeb, M. P. Witter, E. I. Moser, M. B. Moser, Finite scale of spatial representation in the hippocampus. *Science* **321**, 140–143 (2008).
37. M. W. Jung, S. I. Wiener, B. L. McNaughton, Comparison of spatial firing characteristics of units in dorsal and ventral hippocampus of the rat. *J. Neurosci.* **14**, 7347–7356 (1994).
38. M. W. Jung, H. Lee, Y. Jeong, J. W. Lee, I. Lee, Remembering rewarding futures: A simulation-selection model of the hippocampus. *Hippocampus* **28**, 913–930 (2018).
39. A. A. Carey, Y. Tanaka, M. A. A. van der Meer, Reward revaluation biases hippocampal replay content away from the preferred outcome. *Nat. Neurosci.* **22**, 1450–1459 (2019).
40. Skaggs, B. L. McNaughton, K. M. Gothard, E. J. Markus, An information-theoretic approach to deciphering the hippocampal code, in *Proceedings of the 5th International Conference on Neural Information Processing Systems* (NIPS, 1992), pp. 1030–1037.
41. I. Lee, A. L. Griffin, E. A. Zilli, H. Eichenbaum, M. E. Hasselmo, Gradual translocation of spatial correlates of neuronal firing in the hippocampus toward prospective reward locations. *Neuron* **51**, 639–650 (2006).
42. I. Lee, D. Yoganarasimha, G. Rao, J. J. Knierim, Comparison of population coherence of place cells in hippocampal subfields CA1 and CA3. *Nature* **430**, 456–459 (2004).
43. K. Zhang, I. Ginzburg, B. L. McNaughton, T. J. Sejnowski, Interpreting neuronal population activity by reconstruction: Unified framework with application to hippocampal place cells. *J. Neurophysiol.* **79**, 1017–1044 (1998).
44. E. N. Brown, L. M. Frank, D. Tang, M. C. Quirk, M. A. Wilson, A statistical paradigm for neural spike train decoding applied to position prediction from ensemble firing patterns of rat hippocampal place cells. *J. Neurosci.* **18**, 7411–7425 (1998).

Acknowledgments: We thank J. Shin for conducting some pilot experiments for this study and aiding in collecting electrophysiological data. **Funding:** This study was supported by the National Research Foundation of Korea (NRF 2018R1A4A1025616, 2019R1A2C2088799, 2021R1A4A2001803, and 2022M3E5E8017723 to I.L. and NRF 2022R1I1A1A0106893511 to S.-W.J.) and the Ministry of Education of Korea (BK21 FOUR to I.L.). **Author contributions:** Conceptualization: I.L. and S.-W.J. Methodology: I.L. and S.-W.J. Software: S.-W.J. and H.-S.H. Investigation: I.L. and S.-W.J. Formal analysis: S.-W.J. and H.-S.H. Resources: I.L. and S.-W.J. Validation: I.L., S.-W.J., and H.-S.H. Visualization: I.L., S.-W.J., and H.-S.H. Data curation: S.-W.J. and H.-S.H. Supervision: I.L. Writing—original draft: I.L. and S.-W.J. Writing—review and editing: I.L., S.-W.J., and H.-S.H. Project administration: I.L. Funding acquisition: I.L. and S.-W.J. **Competing interests:** The other authors declare that they have no competing interests. **Data and materials availability:** All data needed to evaluate the conclusions in the paper are present in the paper and/or the Supplementary Materials.

Submitted 19 November 2023
Accepted 26 June 2024
Published 7 August 2024
10.1126/sciadv.adn0416